Modeling the wave phenomena in acoustic and elastic media with sharp variations of physical properties using the grid-characteristic method

Alena V. Favorskaya,[1] Michael S. Zhdanov,[1,2,3] Nikolay I. Khokhlov[1], and Igor B. Petrov[1]

[1]Laboratory of Computational Geophysics, Moscow Institute of Physics and Technology, Moscow, Russia.

[2]Department of Geology and Geophysics, University of Utah, Salt Lake City, UT, USA.

[3]TechnoImaging, Salt Lake City, UT, USA

Corresponding author
Alena V. Favorskaya
aleanera@yandex.ru, Moscow Institute of Physics and Technology, Laboratory of Computational Geophysics, 9, Institutsky Pereulok st., Dolgoprudny, Moscow Region, 141700 Russian Federation

This article has been accepted for publication and undergone full peer review but has not been through the copyediting, typesetting, pagination and proofreading process, which may lead to differences between this version and the Version of Record. Please cite this article as doi: 10.1111/1365-2478.12639

ABSTRACT

This paper introduces a novel method of modeling acoustic and elastic wave propagation in inhomogeneous media with sharp variations of physical properties based on the recently developed grid-characteristic method which considers different types of waves generated in inhomogeneous linear elastic media (e.g., longitudinal, transverse, Stoneley, Rayleigh, scattered PP-, SS-waves, and converted PS- and SP-waves). In the framework of this method, the problem of solving acoustic or elastic wave equations is reduced to the interpolation of the solutions, determined at earlier time, thus avoiding a direct solution of the large systems of linear equations required by the FD or FE methods. We apply the grid-characteristic method to compare wave phenomena computed using the acoustic and elastic wave equations in geological medium containing a hydrocarbon reservoir or a fracture zone. The results of this study demonstrate that the developed algorithm can be used as an effective technique for modeling wave phenomena in the models containing hydrocarbon reservoir and/or the fracture zones, which are important targets of seismic exploration.

Key words: Acoustics, Elastics, Wave phenomena, Modelling, Fracture zone.

INTRODUCTION

Numerical modeling of seismic wave propagation is often based on acoustic wave approximation (Aki and Richards 2002; Bording and Lines 1997; Chapman 2004). The three most common types of modeling methods in use in geophysics are direct methods, integral-equation methods, and asymptotic methods (Carcione, Herman and Kroode 2002). Over the last decade significant progress has been made in all these methods (Wang and Liu 2007; Etgen and O'Brien 2007; Hestholm 2009; Tong, Yang and Hua 2011; Di Bartolo, Dors and Mansur 2012; Hobro, Chapman and Robertsson 2014; Sanyi *et al.* 2014).

However, the actual wave propagation processes in geological media can be more accurately represented by elastic wave equations. The solution of this problem has been discussed in numerous publications. For example, in the papers by Levander (1988), Seriani *et al.* (1992), and Van Vossen, Robertsson and Chapman (2002), the authors presented solutions based on the finite element method, while Jianfeng (1997), Zhang, Zhang and Chen (2012), and many others used a finite-difference method. Käser and Igel (2001) simulated 2D wave propagation on unstructured grids using explicit differential operators, and Käser and Dumbser (2006a,b; 2008) applied a discontinuous Galerkin method. Zeng and Liu (2004) suggested a multidomain pseudospectral time domain-method based on the spectral derivative operator approximated by Chebyshev or Lagrange polynomials. Peter *et al.* (2011) used a spectral-element method on unstructured hexahedral meshes for numerical simulation in both elastic and acoustic media. A comprehensive review of the modern methods of modeling seismic wave propagation can be found in Virieux *et al.* (2012). A hybrid acoustic-elastic modeling method based on adaptive grid finite-difference scheme was suggested by Jiang and Jin (2013). Di Bartolo *et al*. (2015) discussed a memory optimized acoustic-elastic finite-difference coupling approach, while Matuszyk and Demkowicz (2014) solved a coupled

poroelastic, acoustic and elastic wave propagation problems using automatic hp-adaptivity method.

The validity of the acoustic approximation for elastic waves in heterogeneous media was investigated recently by Solano, Stopin and Plessix (2013) and Cance and Capdeville (2015).

A novel approach to modeling wave phenomena based on the grid-characteristic method (GCM, Magomedov and Kholodov, 1988) was developed in Petrov *et al.* (2013), Golubev, Petrov and Khokhlov (2013a, b), Muratov and Petrov (2013), Kvasov and Petrov (2012), and Favorskaya *et al.* (2014). The GCM approach is based on a linear transformation of the original hyperbolic system of equations, describing the wave phenomena in acoustic or elastic media, into a system of transport equations, for which the solution at later time can be determined as a linear combination of the displaced at the certain spatial-step solutions at some previous time moment. Therefore, the problem of solving acoustic or elastic wave equations is reduced to the interpolation of the solutions, determined at earlier time, thus avoiding a direct solution of the large system of linear equations, usually required in the framework of the conventional finite-difference modeling. The interpolation problem can be solved using an arbitrary grid (e.g., regular, irregular, triangular, tetrahedral, curvilinear, etc.), which allows us to correctly represent a complex medium by using a fine grid near inhomogeneities and a course grid away from the sources and/or inhomogeneities. We should note that, the method can be used to model the wave propagation in lossy media as well; however, in this paper we will consider the nondispersive media only. The comparison between GCM approach and the other forward modeling techniques was discussed in Biryukov *et al.* 2016.

In this paper, we demonstrate that, by using the GCM approach and the correct boundary conditions on the interfaces and boundaries of the modeling domain, one can model the wave phenomena in the acoustic and elastic media, by producing the results, which

represent all complexity of the waves propagation with different types of the waves present (e.g., longitudinal, transverse, Stoneley, Rayleigh, scattered PP-, SS-waves, and converted PS- and SP-waves).

This paper uses the advantages of the GCM approach to compare the wave patterns and the seismograms obtained using the numerical modeling of the wave propagation based on acoustic and elastic wave equations, respectively. Thus, we demonstrate significant differences in seismic responses produced by the two different modeling approaches. These differences indicate that the conventional inversion algorithms based on an acoustic model of the seismic wave propagation may provide erroneous results in interpretation of the seismic data.

Note that, one of the major problems related to modeling the wave phenomenon is an accurate calculation of the elastic and/or acoustic waves in a medium with sharp physical contrasts, e.g., oil-water interface and/or fracture zones. In the current paper, we demonstrate how the GCM approach can be used for solving this problem. As an example, we present the results of modeling the acoustic wave propagation in the medium with a hydrocarbon (HC) reservoir and with several fractures characterized by sharp variations of elastic properties. The last problem is important in applications in shale-gas industry related to hydraulic fracture monitoring.

We begin this paper with a summary of the basic principles of the GCM technique and present the recent developments in application of this method for solving both the elastic and acoustic wave equations.

ELASTIC AND ACOUSTIC WAVE EQUATIONS

The basic equations of motion of the linear-elastic medium can be written as follows (Aki and Richards 2002; LeVeque 2002; Zhdanov 2002, 2015):

$$\rho \mathbf{v}_t = (\nabla \cdot \mathbf{T})^{\mathrm{T}}, \tag{1}$$

$$\mathbf{T} = \lambda(\nabla \cdot \mathbf{v})\mathbf{I} + \mu(\nabla \otimes \mathbf{v} + (\nabla \otimes \mathbf{v})^{\mathrm{T}}), \quad (2)$$

where ρ is density, $\mathbf{v}$ is velocity, $\mathbf{T}$ is the stress tensor, and λ, μ are the Lamé parameters, characterizing the elastic properties of the medium.

We use the following mathematical notations throughout this paper:

$\mathbf{a}_t \equiv \frac{\partial a}{\partial t}$ is the partial derivative of field $\mathbf{a}$ with respect to time t;

$\mathbf{a}\otimes\mathbf{b}$ is a tensor product of two vectors, $\mathbf{a}$ and $\mathbf{b}$, $(\mathbf{a}\otimes\mathbf{b})_{ij} = a_i b_j$;

$\mathbf{I}$ is identity tensor of rank 2.

The system of equations describing the acoustic wave propagation can be written as follows (Landau and Lifshitz 1959; Aki and Richards 2002; LeVeque 2002; Zhdanov 2002, 2015):

$$\rho \mathbf{v}_t = -\nabla p, \quad (3)$$

$$p_t = -c^2 \rho(\nabla \cdot \mathbf{v}), \quad (4)$$

where p is an acoustic pressure field in the medium, $\mathbf{v}$ is the velocity of the acoustic wave propagation, and c is the speed of the sound in the acoustic medium. Note that, equations (3) and (4) hold for acoustic wave propagation within incompressible fluid as well.

THE GRID-CHARACTERISTIC METHOD FOR NUMERICAL MODELING ELASTIC WAVES IN INHOMOGENEOUS MEDIUM

The grid-characteristic method (GCM) uses the characteristic properties of the systems of hyperbolic equations, describing the elastic wave propagation (Petrov *et al.* 2013; Golubev *et al*. 2013). The mathematical principles of the GCM approach are summarized in Appendix A. It is based on representing the equations of motion of the linear-elastic medium in the following form:

$$\mathbf{q}_t + \mathbf{A}_1\mathbf{q}_x + \mathbf{A}_2\mathbf{q}_y + \mathbf{A}_3\mathbf{q}_z = 0. \quad (5)$$

In the last equation, $\mathbf{q}$ is a vector of unknown fields, having 9 components and equal to

$$\mathbf{q} = \begin{bmatrix} \mathbf{v} \\ \mathbf{T} \end{bmatrix} = [v_1 \quad v_2 \quad v_3 \quad T_{11} \quad T_{22} \quad T_{33} \quad T_{23} \quad T_{13} \quad T_{12}]^{\mathrm{T}}. \tag{6}$$

where $\mathbf{q}(t, x, y, z)$ is a vector of the unknown fields; $\mathbf{q}_t$ denotes the partial derivative of $\mathbf{q}$ with respect to t; $\mathbf{q}_x$, $\mathbf{q}_y$ and $\mathbf{q}_z$ denote the partial derivatives of vector $\mathbf{q}$ with respect to x , y, and z, respectively.

Matrices $\mathbf{A}_k$, $k = 1,2,3$, are the 9×9 matrices given by the following expression:

$$\mathbf{A}_1 = -\begin{bmatrix} 0 & 0 & 0 & \rho^{-1} & 0 & 0 & 0 & 0 & 0 \\ 0 & 0 & 0 & 0 & 0 & 0 & 0 & 0 & \rho^{-1} \\ 0 & 0 & 0 & 0 & 0 & 0 & 0 & \rho^{-1} & 0 \\ \lambda+2\mu & 0 & 0 & 0 & 0 & 0 & 0 & 0 & 0 \\ \lambda & 0 & 0 & 0 & 0 & 0 & 0 & 0 & 0 \\ \lambda & 0 & 0 & 0 & 0 & 0 & 0 & 0 & 0 \\ 0 & 0 & 0 & 0 & 0 & 0 & 0 & 0 & 0 \\ 0 & 0 & \mu & 0 & 0 & 0 & 0 & 0 & 0 \\ 0 & \mu & 0 & 0 & 0 & 0 & 0 & 0 & 0 \end{bmatrix}, \tag{7}$$

matrix $\mathbf{A}_2$ is given by the following expression:

$$\mathbf{A}_2 = -\begin{bmatrix} 0 & 0 & 0 & 0 & 0 & 0 & 0 & 0 & \rho^{-1} \\ 0 & 0 & 0 & 0 & \rho^{-1} & 0 & 0 & 0 & 0 \\ 0 & 0 & 0 & 0 & 0 & 0 & \rho^{-1} & 0 & 0 \\ 0 & \lambda & 0 & 0 & 0 & 0 & 0 & 0 & 0 \\ 0 & \lambda+2\mu & 0 & 0 & 0 & 0 & 0 & 0 & 0 \\ 0 & \lambda & 0 & 0 & 0 & 0 & 0 & 0 & 0 \\ 0 & 0 & \mu & 0 & 0 & 0 & 0 & 0 & 0 \\ 0 & 0 & 0 & 0 & 0 & 0 & 0 & 0 & 0 \\ \mu & 0 & 0 & 0 & 0 & 0 & 0 & 0 & 0 \end{bmatrix}, \tag{8}$$

and matrix $\mathbf{A}_3$ can be written as follows:

$$\mathbf{A}_3 = -\begin{bmatrix} 0 & 0 & 0 & 0 & 0 & 0 & 0 & \rho^{-1} & 0 \\ 0 & 0 & 0 & 0 & 0 & 0 & \rho^{-1} & 0 & 0 \\ 0 & 0 & 0 & 0 & 0 & \rho^{-1} & 0 & 0 & 0 \\ 0 & 0 & \lambda & 0 & 0 & 0 & 0 & 0 & 0 \\ 0 & 0 & \lambda & 0 & 0 & 0 & 0 & 0 & 0 \\ 0 & 0 & \lambda+2\mu & 0 & 0 & 0 & 0 & 0 & 0 \\ 0 & \mu & 0 & 0 & 0 & 0 & 0 & 0 & 0 \\ \mu & 0 & 0 & 0 & 0 & 0 & 0 & 0 & 0 \\ 0 & 0 & 0 & 0 & 0 & 0 & 0 & 0 & 0 \end{bmatrix}. \tag{9}$$

The product of matrix $\mathbf{A}_k$ and vector $\mathbf{q}$ can be calculated as follows:

$$\mathbf{A}_k \begin{bmatrix} \mathbf{v} \\ \mathbf{T} \end{bmatrix} = -\begin{bmatrix} \rho^{-1}(\mathbf{T} \cdot \mathbf{n}) \\ \lambda(\mathbf{v} \cdot \mathbf{n})\mathbf{I} + \mu(\mathbf{n} \otimes \mathbf{v} + \mathbf{v} \otimes \mathbf{n}) \end{bmatrix}, \tag{10}$$

where $\otimes$ denotes the tensor product of two vectors.

In the last equation $\mathbf{n}$ is a unit vector directed along the $\mathbf{x}$, $\mathbf{y}$, or $\mathbf{z}$ directions for matrices $\mathbf{A}_1$, $\mathbf{A}_2$, or $\mathbf{A}_3$, respectively.

As we discussed above, the GCM approach is based on representing the solutions of the acoustic and/or elastic wave equations at later time as a linear combination of the displaced at a certain spatial step solutions at some previous time moment. This representation can be used to construct a direct time-stepping iterative algorithm of computing the wave fields at any time moment from the initial and boundary conditions. In order to develop this time-stepping formula, we represent matrices $\mathbf{A}_k$ using their spectral decomposition. For example, for matrix $\mathbf{A}_1$ we have:

$$\mathbf{A}_1 = (\mathbf{\Omega}_1)^{-1}\mathbf{\Lambda}_1\mathbf{\Omega}_1, \tag{11}$$

where $\mathbf{\Lambda}_1$ is a 9×9 diagonal matrix, formed by the eigenvalues of matrix $\mathbf{A}_1$; and $(\mathbf{\Omega}_1)^{-1}$ is a 9×9 matrix formed by the corresponding eigenvectors. Note that, matrices $\mathbf{A}_1$, $\mathbf{A}_2$ and $\mathbf{A}_3$ have the same set of eigenvalues:

$$\{c_\mathrm{p}, -c_\mathrm{p}, c_\mathrm{s}, -c_\mathrm{s}, c_\mathrm{s}, -c_\mathrm{s}, 0,0,0\}. \tag{12}$$

In the last formula, c_p is a P-wave velocity being equal to $\left(\rho^{-1}(\lambda + 2\mu)\right)^{1/2}$ and c_s is an S-wave velocity being equal to $(\rho^{-1}\mu)^{1/2}$.

Let us consider some direction $\mathbf{x}$. We assume that the unit vector $\mathbf{n}$ is directed along this direction, while the unit vectors $\mathbf{n}_1$ and $\mathbf{n}_2$ form a Cartesian basis together with $\mathbf{n}$. We also introduce the following symmetric tensors of rank 2:

$$\mathbf{N}_{ij} = \frac{1}{2}\left(\mathbf{n}_i \otimes \mathbf{n}_j + \mathbf{n}_j \otimes \mathbf{n}_i\right), \tag{13}$$

where indices i and j vary from 0 to 2 in order to simplify the final formulas, and $\mathbf{n}_0 = \mathbf{n}$.

It is shown in Appendix A that, the solution of equation (5), vector **q,** along the *x*, *y*, and *z* directions can be written as follows:

$$\mathbf{q}(t+\tau,x,y,z) = \sum_{j=1}^{J} \mathbf{X}_{1,j}\mathbf{q}\big(t, x-\Lambda_{1,j}\tau, y, z\big),$$

$$\mathbf{q}(t+\tau,x,y,z) = \sum_{j=1}^{J} \mathbf{X}_{2,j}\mathbf{q}\big(t, x, y-\Lambda_{2,j}\tau, z\big), \quad (14)$$

$$\mathbf{q}(t+\tau,x,y,z) = \sum_{j=1}^{J} \mathbf{X}_{3,j}\mathbf{q}\big(t, x, y, z-\Lambda_{3,j}\tau\big).$$

Here τ is the time step of the solution, and $\mathbf{X}_{1,j}$, $\mathbf{X}_{2,j}$ and $\mathbf{X}_{3,j}$ are the characteristic matrices expressed through the components of matrices $\mathbf{A}_1$, $\mathbf{A}_2$ and $\mathbf{A}_3$ and their eigenvalues as follows:

$$\mathbf{X}_{\mathrm{i},j} = \boldsymbol{\varpi}_{*i,j}\boldsymbol{\varpi}_{i,j},\ i=1,2,3; \quad (15)$$

where $\boldsymbol{\varpi}_{*i,j}$ is the j's column of matrix $(\boldsymbol{\Omega}_\mathrm{i})^{-1}$, and $\boldsymbol{\varpi}_{i,\mathrm{j}}$ is the j's row of matrix $\boldsymbol{\Omega}_\mathrm{i}$. The scalar components of the column matrices $\boldsymbol{\varpi}_{*\mathrm{i,j}}$ are defined by the following expressions:

$$\omega_{1,2} = \left(\boldsymbol{\Omega}_1 \begin{bmatrix}\mathbf{v}\\ \mathbf{T}\end{bmatrix}\right)_{1,2} = \mathbf{n}\cdot\mathbf{v} \mp \left(c_\mathrm{p}\rho\right)^{-1}(\mathbf{N}_{00} * \mathbf{T}), \quad (16)$$

$$\omega_{3,4} = \mathbf{n}_1\cdot\mathbf{v} \mp (c_\mathrm{s}\rho)^{-1}(\mathbf{N}_{01} * \mathbf{T}), \quad (17)$$

$$\omega_{5,6} = \mathbf{n}_2\cdot\mathbf{v} \mp (c_\mathrm{s}\rho)^{-1}(\mathbf{N}_{02} * \mathbf{T}), \quad (18)$$

$$\omega_7 = \mathbf{N}_{12} * \mathbf{T}, \quad (19)$$

$$\omega_8 = (\mathbf{N}_{11} - \mathbf{N}_{22}) * \mathbf{T}, \quad (20)$$

$$\omega_9 = \left(\mathbf{N}_{11} + \mathbf{N}_{22} - \frac{2\lambda}{\lambda+2\mu}\mathbf{N}_{00}\right) * \mathbf{T}. \quad (21)$$

In equations (16) - (21) the asterisk "*"denotes the convolution of two tensors of rank 2. Expressions (14) can be used to find the solution, vector $\mathbf{q}$, at any time moment, $t+\tau$, from the given initial conditions, thus representing a direct time-stepping algorithm of numerical modeling the elastic wave propagation in inhomogeneous media.

In order to accurately take into account the conditions on the boundary of the modeling domain and on the interfaces inside the modeling domain between the elastic bodies with different properties, we use the corresponding boundary and interface conditions, discussed in Appendix B.

We should note in conclusion of this section that, because the GCM is based on the solution of the fundamental equations of motion of the linear-elastic medium, (1) and (2), it takes into account all varieties of the waves generated in inhomogeneous medium (e.g., longitudinal, transverse, Stoneley, Rayleigh, scattered PP-, SS-waves, and converted PS- and SP-waves).

THE GRID-CHARACTERISTIC METHOD FOR NUMERICAL WAVE MODELING IN ACOUSTIC MEDIUM

We use the grid-characteristic method (GCM) for numerical wave modeling in an acoustic medium as well. In the case of acoustic waves, vector $\mathbf{q}$ of unknown fields has four components, and it is equal to the following expression:

$$\mathbf{q} = \begin{bmatrix} \mathbf{v} \\ p \end{bmatrix} = [v_1 \quad v_2 \quad v_3 \quad p]^{\mathrm{T}}. \tag{22}$$

In acoustic case, matrices $\mathbf{A}_k$, $k = 1,2,3,$ become $[4\times 4]$ matrices given by the following formulas:

$$\mathbf{A}_1 = -\begin{bmatrix} 0 & 0 & 0 & \rho^{-1} \\ \rho c^2 & 0 & 0 & 0 \\ \rho c^2 & 0 & 0 & 0 \\ \rho c^2 & 0 & 0 & 0 \end{bmatrix}, \tag{23}$$

$$\mathbf{A}_2 = -\begin{bmatrix} 0 & 0 & 0 & \rho^{-1} \\ 0 & \rho c^2 & 0 & 0 \\ 0 & \rho c^2 & 0 & 0 \\ 0 & \rho c^2 & 0 & 0 \end{bmatrix}, \tag{24}$$

$$\mathbf{A}_3 = -\begin{bmatrix} 0 & 0 & 0 & \rho^{-1} \\ 0 & 0 & \rho c^2 & 0 \\ 0 & 0 & \rho c^2 & 0 \\ 0 & 0 & \rho c^2 & 0 \end{bmatrix}. \tag{25}$$

The product of matrix $\mathbf{A}_k$ and vector $\mathbf{q}$ can be calculated as follows:

$$\mathbf{A}_k \begin{bmatrix} \mathbf{v} \\ p \end{bmatrix} = \begin{bmatrix} \rho^{-1} p \mathbf{n} \\ c^2 \rho (\mathbf{n} \cdot \mathbf{v}) \end{bmatrix}. \tag{26}$$

In the last equation, $\mathbf{n}$ is a unit vector directed along the $\mathbf{x}$, $\mathbf{y}$, or $\mathbf{z}$ directions for matrices $\mathbf{A}_1$, $\mathbf{A}_2$, or $\mathbf{A}_3$, respectively. Note that matrices $\mathbf{A}_1$, $\mathbf{A}_2$ and $\mathbf{A}_3$ have the same set of the eigenvalues:

$$\{c, -c, 0, 0\}. \tag{27}$$

The scalar components, ω_j, of vector $\boldsymbol{\omega}(t, x, y, z)$ from equation (A8), which is the product of matrix $\boldsymbol{\Omega}_1$ and vector $\mathbf{q}$, can be written as follows:

$$\omega_{1,2} = \left(\boldsymbol{\Omega}_1 \begin{bmatrix} \mathbf{v} \\ p \end{bmatrix} \right)_{1,2} = \mathbf{n} \cdot \mathbf{v} \pm \left(c_\mathrm{p} \rho \right)^{-1} p, \tag{28}$$

$$\omega_3 = \mathbf{n}_1 \cdot \mathbf{v}, \tag{29}$$

$$\omega_4 = \mathbf{n}_2 \cdot \mathbf{v}. \tag{30}$$

Substituting expressions (28) – (30) for scalar components ω_j, in equations (14), we arrive at the direct time-stepping algorithm of numerical modeling the elastic wave propagation in inhomogeneous media.

We also use the corresponding boundary and interface conditions for acoustic waves, discussed in Appendix B.

NUMERICAL COMPARISON OF THE GRID-CHARACTERISTIC METHOD WITH THE EXACT METHOD

We have conducted a standard test for validating the grid-characteristic method using a classical Lamb problem (Lamb 1904). In this problem, a wavefield is modeled for a point source of a vertical force located under a free boundary (see at Figure 1).. A two-dimensional solution of this problem can be calculated analytically (Berg *et al.* 1994). The parameters of the model were selected close to those of Dumbser, K¨aser and De La Puente (2000).

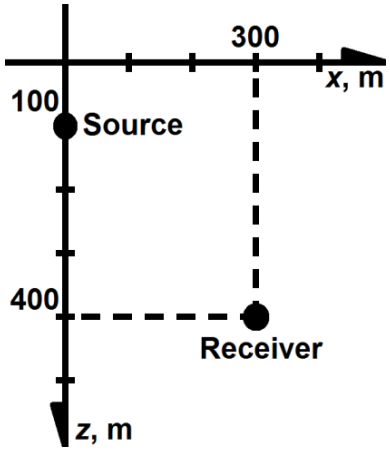

Figure 1. A sketch of a Lamb test model.

The problem was considered in an isotropic elastic medium with a P-wave velocity equal to 3200 m/s, the S-wave velocity of 1847.5 m/s, the density of the medium was assumed to be equal to 2200 kg/m^3. The positions of the source and receiver are shown in Figure 1 ((0 m, 100 m), and (300 m, 400 m), respectively). The waveform of the pulse in the source was given by a Riker impulse with a frequency of 14.5 Hz. We used a two-dimensional regular grid with a coordinate step of 4 m, and with the total number of nodes equal to 700 x 500. The integration time step was equal to 5 ms, with the total time of 1 s, thus requiring 2,000 time steps. The numerical integration was done using a computational scheme of the third order of accuracy. Figure 2 presents the seismograms obtained numerically using the GCM and analytically. One can see from this Figure that, there is a good match between the solutions and the difference between the analytical and the numerical solutions is also very small.

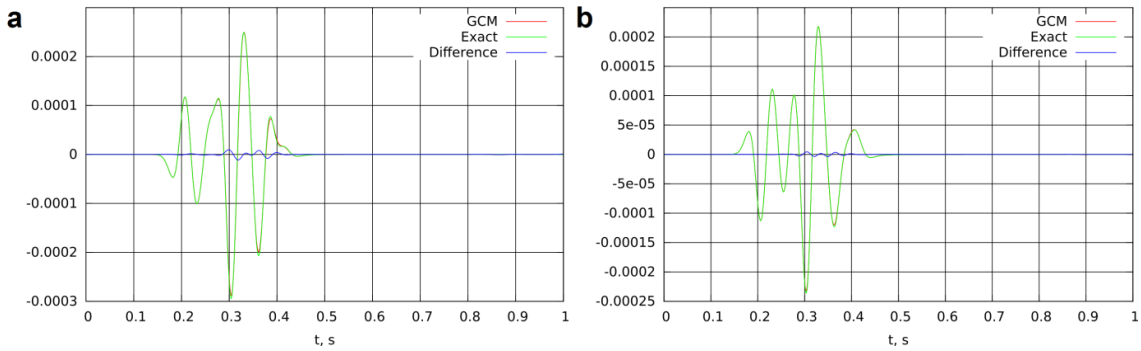

Figure 2. Seismograms obtained numerically using the grid-characterisitic method and analytically for the Lamb test model. Panel (a) – horizontal component of the velocity. Panel (b) – vertical component of the velocity.

The next test is the validation of the realization of the contact condition between the two elastic media with different seismic parameters. In this test, two elastic half spaces and a compressional point source were considered. The solution of this problem can be calculated analytically as well (Berg *et al.* 1994). We considered two half spaces with the interface passing along coordinate z = 0 (Figure 3). The source and the receiver are located in the lower half space, in the points with coordinates of (0 m, 100 m) and (300 m, 400 m), respectively. The medium in the upper half space is characterized by P-wave velocity equal to 2500 m/s, S-wave velocity 1558 m/s, and the density of the medium was 1500 kg/m^3. The medium in the lower half space is assumed having P-wave velocity equal to 3400 m/s, S-wave velocity of .484 m/s, and the density of 2600 kg/m^3. The waveform of the pulse in the source was given by a Riker impulse with a frequency of 14.5 Hz. We used a two-dimensional regular grid with a coordinate step of 2 m, and a grid size of 1000 x 1500 nodes. Figure 4 shows the corresponding seismograms obtained numerically using the GCM and analytically. The results of this numerical study demonstrate that, the difference between the analytical and the numerical solutions is negligibly small.

Thus, the results of our numerical study demonstrate that the GCM is an accurate numerical technique for simulating the elastic wavefields. Our test models were relatively

simple in order to compare the GCM with the analytical solutions. The examples of comparison between GCM and other numerical methods for more complicated models can be found in Biryukov *et al.* (2016).

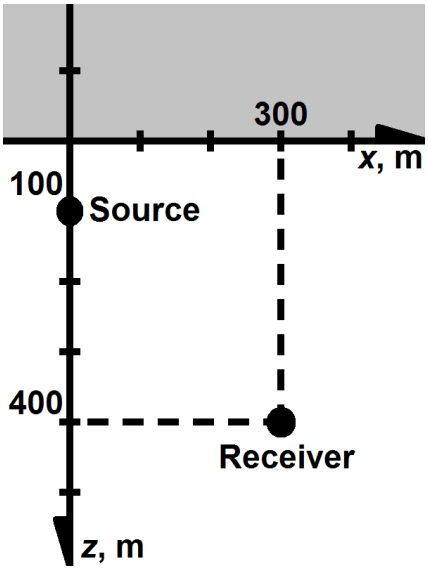

Figure 3. A sketch of two half spaces model.

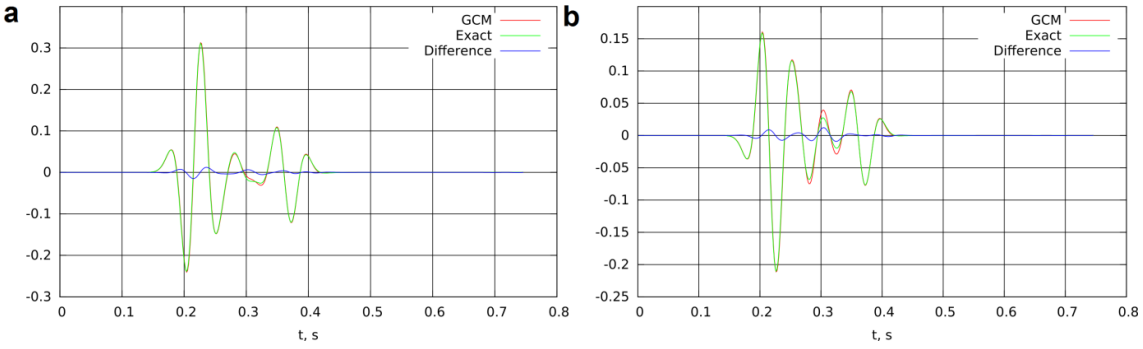

Figure 4. The original seismograms obtained numerically and analytically. for two half spaces model. Panel (a) – horizontal component of the velocity. Panel (b) – vertical component of the velocity.

A NUMERICAL COMPARISON OF THE WAVE PHENOMENA IN ACOUSTIC AND ELASTIC MEDIA

We illustrate the developed numerical method of modeling elastic and acoustic waves by a comparison study of the wave phenomena in acoustic and elastic media.

Let us consider the horizontally-layered model shown in Figure 5. The parameters of each layer are summarized in Table 1. We also assume that layer #7 has a limited horizontal extension to model a hydrocarbon (HC) reservoir with the relatively low velocities of the seismic wave propagation. For simplicity, we consider a 2D model with all parameters varying in the vertical and one horizontal direction only. The modeling domain extends to 12,000 m and 4,001 m in the horizontal and vertical directions, respectively.

Table 1: Parameters of the multilayed medium shown in Fig. 1

The number of the layers	Density, kg/m^3	P-wave velocity, m/s	S-wave velocity, m/s	Thickness, m
1	2100	2600	1100	60
2	2300	3200	1960	70
3	2300	3700	2260	150
4	2400	4000	2450	340
5	2500	4300	2630	360
6	2600	4500	2750	270
7	2300	3200	1700	60
8	2600	4600	2820	80
9	2700	4800	2940	70

10	2800	5400	3300	2601

We use the nonreflecting boundary conditions on the sides and on the bottom of the modeling domain and the free-surface conditions on the earth's surface (Virieux *et al.* 2012; Petrov *et al.* 2013). The source is modeled by using as a boundary condition at seven central points on the earth's surface a Ricker wavelet with the frequency, f, equal to 31 Hz. We also use zero initial conditions for the wave fields.

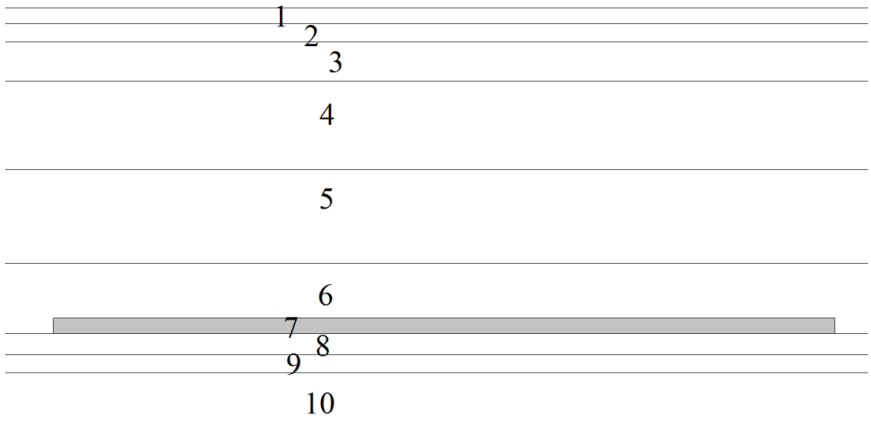

Figure 5. A sketch of a horizontally-layered model, containing a hydrocarbon (HC) reservoir (layer #7) with relatively low velocities of seismic wave propagation.

The sensors (geophones) are located every 24 m along a horizontal profile extended to 4,500 м in both directions from the source. The original systems of the elastic and acoustic wave equations were discretized using a rectangular grid with a cell size of 3 m by 2m in the horizontal and vertical directions, respectively, and the time step was equal to 0.00037 s, with a total time of 1.85 s requiring 5,000 time steps. Note that, the cell size in the bottom layer (#10) was 3 m by 3 m. The computations for the model with the HC reservoir took approximately 10 hours on one computer node (without parallelization). We computer simulated the wave propagation in four different models, described below. *Model 1* represents a horizontally layered elastic medium shown in Figure 1 with the parameters listed in Table 1.

Model 2 is the same as Model 1 with one important difference − this model does not contain inclusion #7 representing an HC reservoir. *Model 3* represents the horizontally layered acoustic medium shown in Figure 1 with the velocities of the acoustic wave propagation equal to the corresponding velocities of the P-wave shown in Table 1. *Model 4* is the same as Model 1 but without inclusion #7 representing the HC reservoir.

Figures 6 and 7 present snapshots of the wave propagations at 0.4514 s and 0.6438 s respectively, with the gray scale representing the amplitude of the wave velocity. Panels (a) in Figures 6 and 7 represent snapshots of the wave propagation in the acoustic medium (Models 3 and 4), while panels (b) show snapshots of the P-wave propagation in the elastic medium (Models 1 and 2). Each panel represents the modeling results for two scenarios -- without (the left side of the panel) and with (the right side of the panel) the HC reservoir (layer #7).

We plot in Figures 8 and 9 the seismograms corresponding to the vertical and horizontal components of the wave velocity, respectively. Panels (a) in Figures 8 and 9 represent seismograms computer simulated for the acoustic medium (Models 3 and 4), while panels (b) plot the corresponding seismograms for the elastic medium (Models 1 and 2). On the left side of each panel we plot the seismograms for the models without the HC reservoir (without layer #7), while on the right side we show the seismograms for the models with the HC reservoir (layer #7).

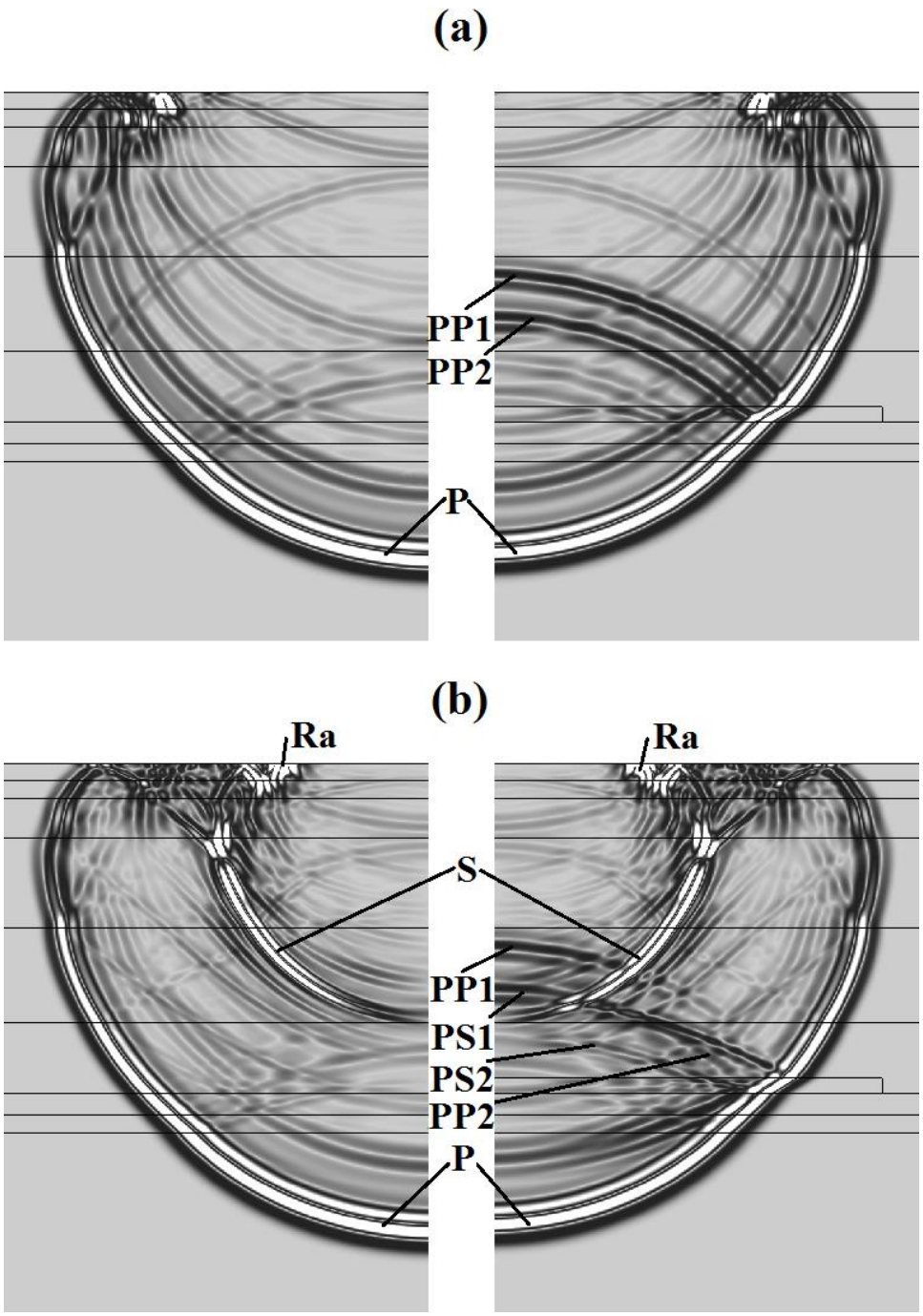

Figure 6. Snapshots of the wave propagations at 0.4514 s with the gray scale representing the amplitude of the wave velocity. Panel (a) represents the wave propagation in the acoustic medium (Models 3 and 4), while panel (b) shows the wave propagation in the elastic medium (Models 1 and 2). The left side of each panel corresponds to the models without the HC reservoir, while the right side corresponds to the models with the HC reservoir.

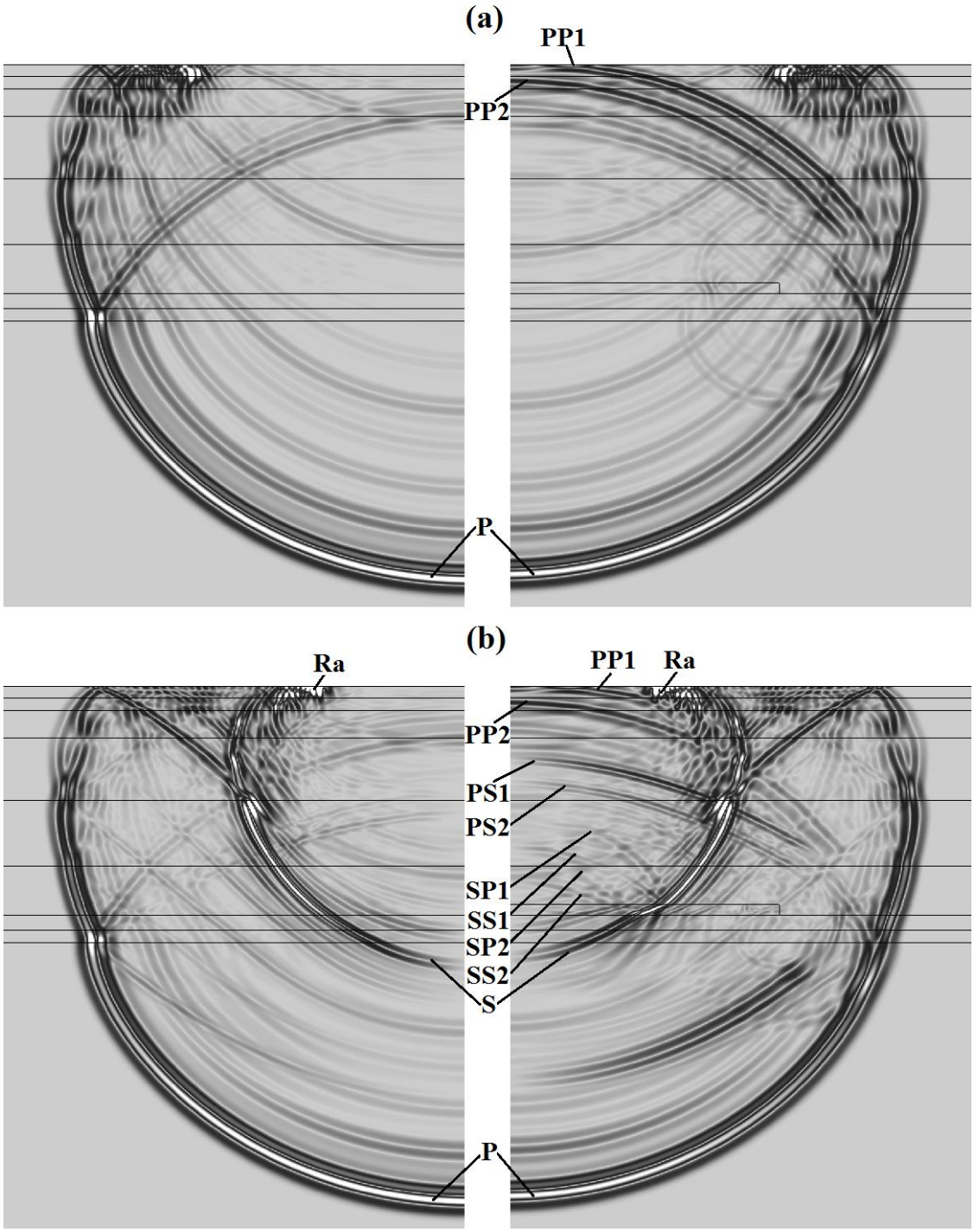

Figure 7. Snapshots of the wave propagations at 0.6438 s with the gray scale representing the amplitude of the wave velocity. Panel (a) represents the wave propagation in the acoustic medium (Models 3 and 4), while panel (b) shows the wave propagation in the elastic medium (Models 1 and 2). The left side of each panel corresponds to the models without the HC reservoir, while the right side corresponds to the models with the HC reservoir.

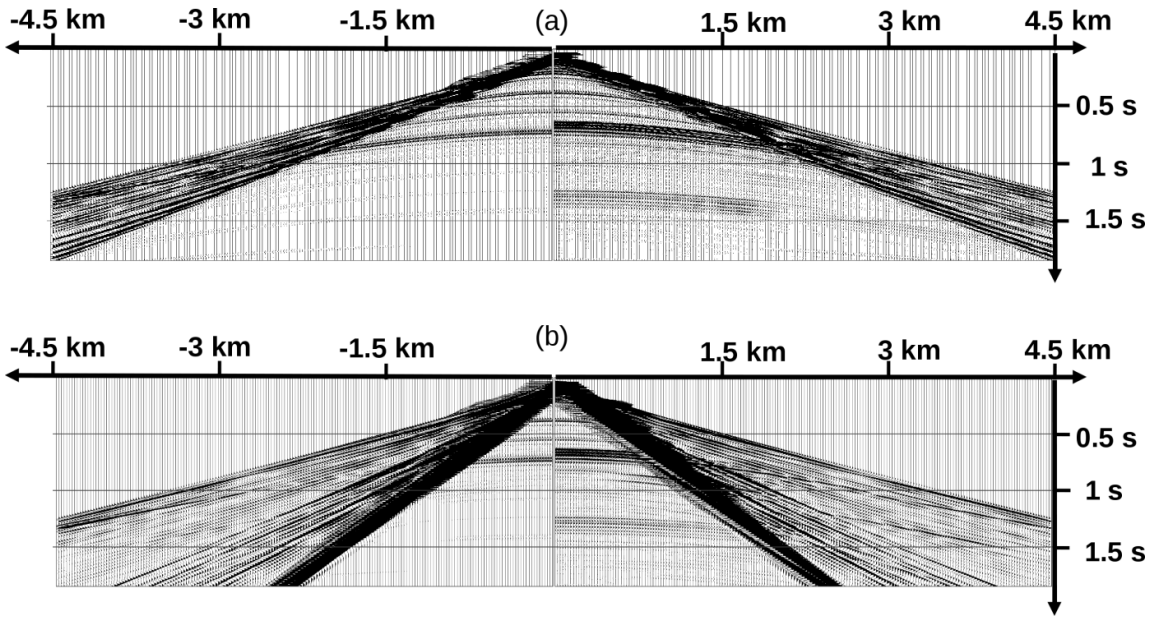

Figure 8. Seismograms corresponding to the vertical component of the wave velocity. Panel (a) represents seismograms computer simulated for the acoustic medium (Models 3 and 4), while panel (b) shows the corresponding seismograms for the elastic medium (Models 1 and 2). The left side of each panel corresponds to the models without the HC reservoir, while the right side corresponds to the models with the HC reservoir. The distance is plotted horizontally. The time is plotted vertically.

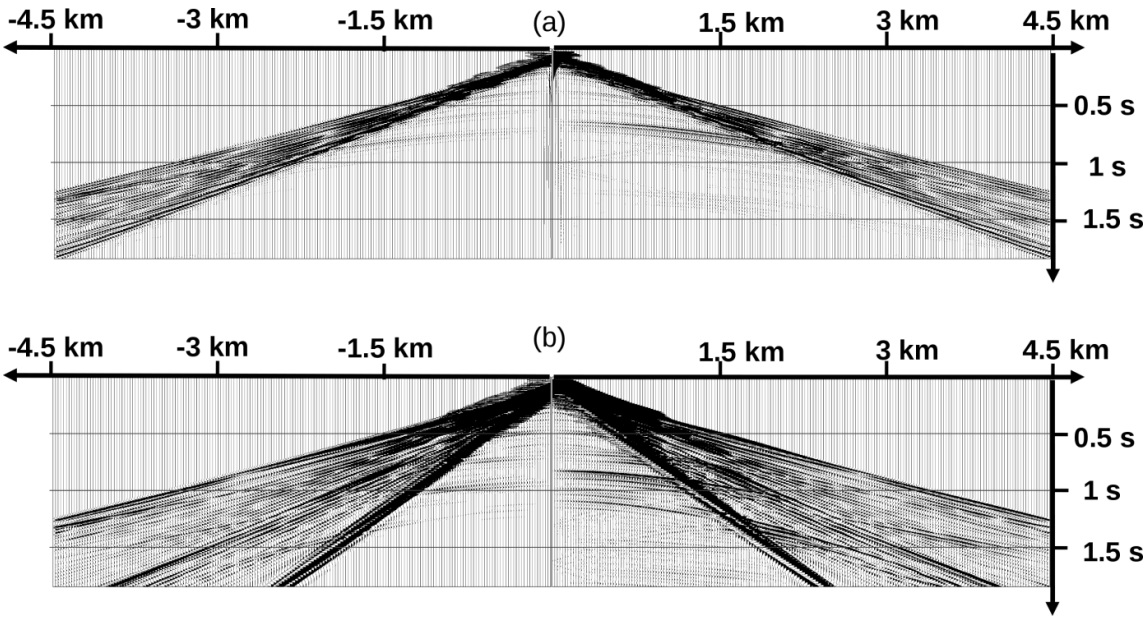

Figure 9. Seismograms corresponding to the horizontal component of the wave velocity. Panel (a) represents seismograms computer simulated for the acoustic medium (Models 3 and 4), while panel (b) shows the corresponding seismograms for the elastic medium (Models 1 and 2). The left side of each panel corresponds to the models without the HC reservoir, while the right side corresponds to the models with the HC reservoir. The distance is plotted horizontally. The time is plotted vertically.

We use the following notations in Figures 6 and 7. Symbol "Ra" marks the Rayleigh waves, symbols "P" and "S" correspond to the P- and S-waves generated by the source. Symbol "PP1" denotes the P-waves, reflected from the top of the HC reservoir, while "PP2" marks the P-waves, reflected from the bottom of the HC reservoir. Symbol "PS1" represents the converted PS-waves reflected from the top of the HC reservoir, while PS2 marks the converted PS-waves reflected from the bottom of the HC reservoir. Symbol "SP1" denotes the converted SP-waves from the top of the reservoir, while "SP2" marks the converted SP-waves from the bottom of the reservoir. Finally, symbols "SS1"and "SS2" denote the converted SS-waves from the top and bottom of the reservoir, respectively.

One can see significant differences in the responses from the hydrocarbon reservoir modeled using the acoustic and wave equations, respectively. Clearly, the wave propagation

in the elastic medium generates an image with much richer wave distribution picture than that produced by the acoustic waves. These figures also illustrate a difference in geometrical pattern and topology of seismic waves for different cases. The converted waves, which are obviously absent in the acoustic model, play the most important role in emphasizing the response from the HC reservoir located in the elastic medium. The Rayleigh waves are also observed in the elastic medium only.

SHARP VARYING SPACE STEPS AND FRACTURE MODELING

The grid-characteristic method GCM approach represents a powerful technique for accurate modeling of the wave phenomena in the presence of sharp physical contrasts, e.g., fracture zones. This is possible because the direct time-stepping algorithm (14) of the GCM can be used for an arbitrary nonumiform grid with a fine discretization near inhomogeneities and a course grid size away from the sources and/or inhomogeneities (e.g., Figure 10). This technique allows us to avoid incorrect oscillations of the solutions which might occur in the case of the use of an uniform grid for the models with sharply varying physical properties.

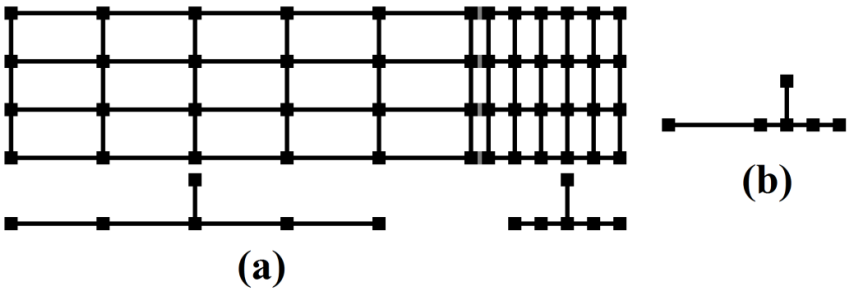

Figure 10. Example of nonuniform grid (a) with different cell sizes in different areas, and nonuniform nodes (b).

The GCM approach could be of particular importance in modeling the wave propagation in the medium containing fractures, e.g., for hydraulic fracture monitoring (HFM). Let us consider a numerical modeling of elastic waves propagating in the

horizontally-layered background model shown in Figure 11 containing sixteen fractures. The parameters of the horizontally layered background model are summarized in Table 2. We also assume that layer #6 contains sixteen fractures with different parameters. The lengths of these fractures are equal to 25 m, 50 m, 25 m, 75 m, 25 m, 50 m, 25 m, 75 m, 25 m, 100 m, 25 m, 75 m, 25 m, 50 m, 25 m, and 25 m, respectively. The width of these fractures is equal to 5 m. For simplicity, we consider a 2D model with all parameters varying in the vertical and one horizontal direction only. The modeling domain extends to 8 400 m and 5 550 m in the horizontal and vertical directions, respectively. For a comparison, we also consider the background model without any fractures. We have applied the GCM based algorithm for computing both the elastic and acoustic waves in this model.

Table 2: Parameters of the horizontally laryed background model shown in Fig. 7

The number of the layer	Density, kg/m^3	P-wave velocity, m/s	S-wave velocity, m/s	Thickness, m
1	2000	2170	674	500
2	2300	2130	795	100
3	2200	2500	1090	300
4	2300	2680	1220	100
5	2400	3000	1385	400
6 (with fractures)	2700	5550	3144	100
7	2800	6000	1250	150
8	2850	6000	1550	4000
Within	1350	2775	1572	–

fractures				

The source and the boundary conditions are the same as in the first experiment. We also use zero initial conditions for the wave fields.

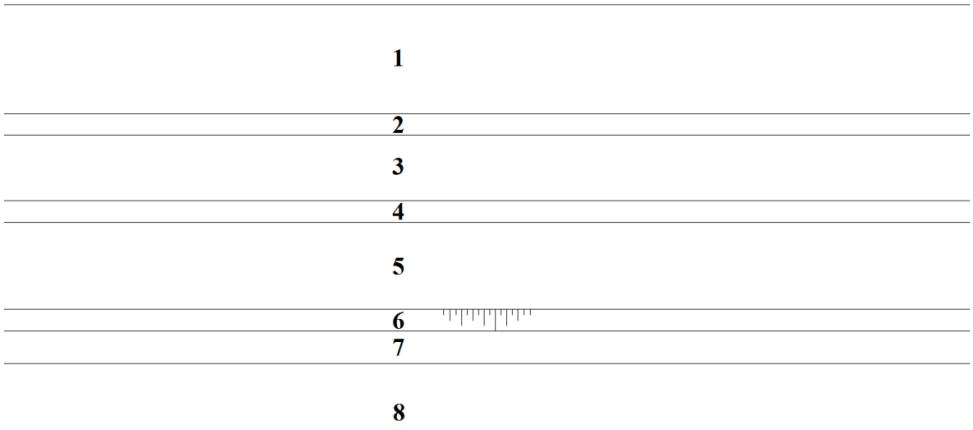

Figure 11. A sketch of a horizontally-layered background model, containing sixteen fractures.

We used a rectangular grid with variable cell size from 5 m to 0.25 m in horizontal and 1 m in vertical directions, respectively, as shown in Figure 12. The time step was equal to 0.00004 s, with a total time of 3 s and with 75,001 time steps. The computations for the model with the fracture zone took approximately 50 hours on one computer node (without parallelization). However, the algorithm of the GCM method is very well suited for parallelization which will speed up all computations significantly. This will be a subject of future research.

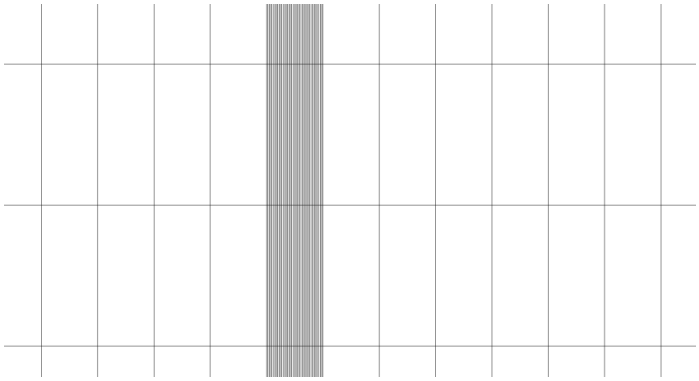

Figure 12. A fragment of the discretization grid used for modeling the wave propagation in the medium with a fracture zone.

Figure 13 presents the snapshots of the wave propagation in the model with the fracture zone (the right side of the figure) and without the fractures (the left side of the figure).

Figure 14 presents right parts of the seismograms computed for a model with fractures. Figure 15 shows right parts of the seismograms representing the difference between seismic signals obtained in the case of fractures and in the case without fracture. Panel (a) represents seismograms computer simulated for the acoustic medium, while panel (b) shows the corresponding seismograms for the elastic medium. The left panels correspond to the horizontal component of the wave velocity, while the right panels correspond to the vertical component of the wave velocity. Note that, the seismogram in the case of acoustic media and horizontal component of velocity is total zero due to the absence of S-waves.

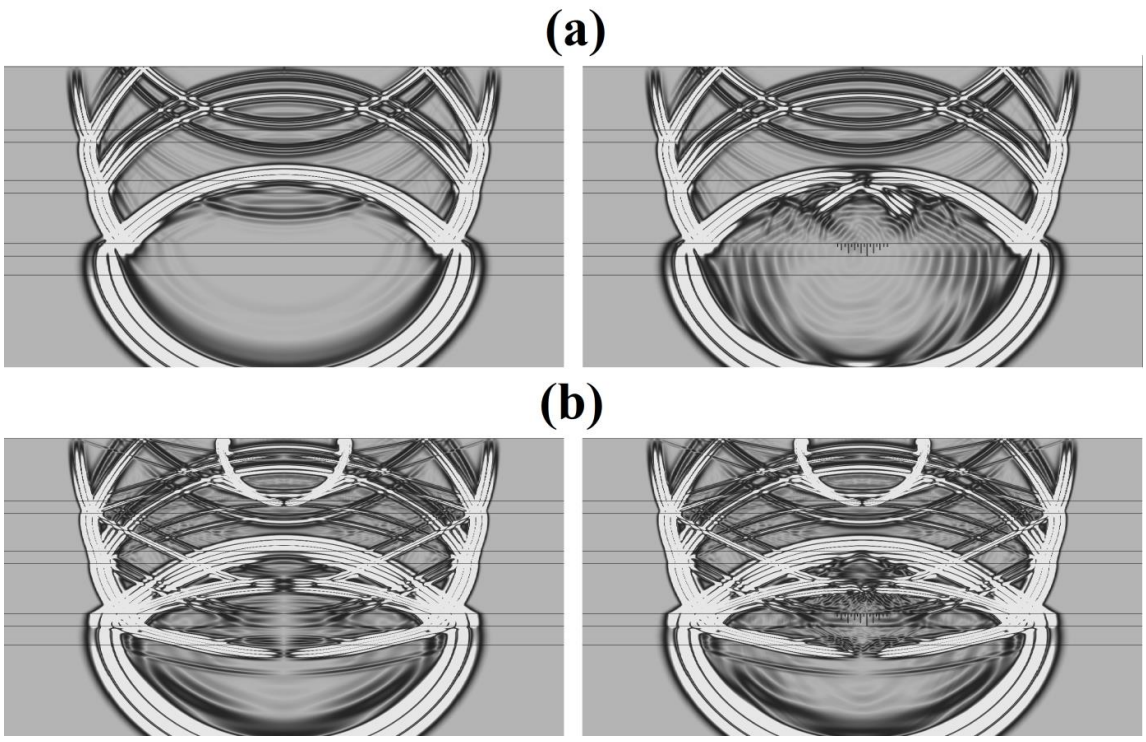

Figure 13. Snapshots of the wave propagations at 0.8 s with the gray scale representing the amplitude of the wave velocity.. Panel (a) represents the wave propagation in the acoustic medium, while panel (b) shows the wave propagation in the elastic medium. The left side of each panel corresponds to the models without any fracture, while the right side corresponds to the models with the fractures.

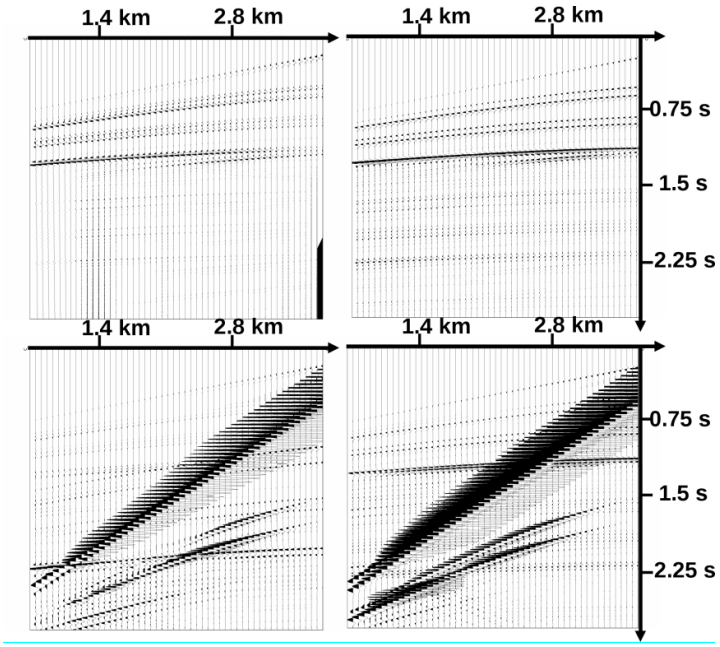

Figure 14. Seismograms representing the seismic signals for a model with fractures. Panel (a) represents seismograms for the acoustic medium, while panel (b) shows the corresponding seismograms for the elastic medium. The left panels correspond to the horizontal component of the wave velocity, while the right panels corresponds to the vertical component of the wave velocity. The distance is plotted horizontally. The time is plotted vertically.

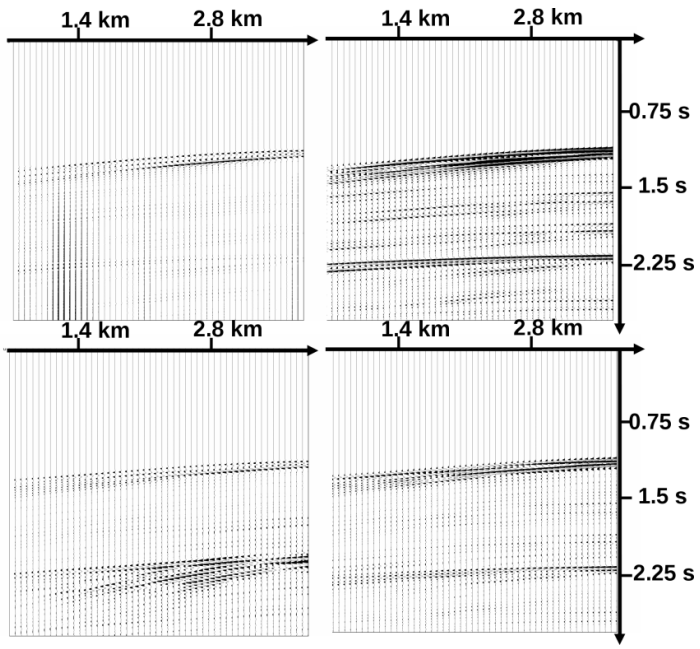

Figure 15. Seismograms representing the difference between seismic signals obtaining in the case of fractures and in the case without any fracture. Panel (a) represents right parts of seismograms computer simulated for the acoustic medium, while panel (b) shows the corresponding right parts of seismograms for the elastic medium. The left side of each panel corresponds to the horizontal component of the wave velocity, while the right side corresponds to the vertical component of the wave velocity. The distance is plotted horizontally. The time is plotted vertically.

CONCLUSIONS

We have presented a novel approach to modeling the wave phenomena in acoustic and elastic media with sharp variations of physical properties using the grid-characteristic method (GCM) and nonregular grids with varying cell sizes near inhomogeneities. This method provides a direct solution of the corresponding systems of acoustic and elastic wave equations in a form of direct time-stepping recursive computations. The advantage of the developed method over the traditional techniques based on the finite difference approximation is that it reduces the problem of solving acoustic or elastic wave equations to the interpolation of the solutions, determined at earlier time, thus avoiding a direct solution of the large system of linear equations, usually required in the framework of the conventional finite-difference

modeling. The GCM approach takes into account all varieties of the waves generated in inhomogeneous medium (e.g., longitudinal, transverse, Stoneley, Rayleigh, scattered PP-, SS-waves, and converted PS- and SP-waves). Using this novel approach, we have conducted a comparison study of the acoustic and elastic wave propagation in the horizontally layered model containing an HC reservoir and a fracture zone. The results of our modeling study have demonstrated that the inclusion of the relatively low velocity layer representing an HC reservoir in the horizontally layered model generates a significantly stronger distortion of the elastic wave distribution than that of the acoustic waves. The same effect occurs in the case of fractures. A distortion of the elastic waves, associated with the HC reservoir or a fracture zone, is manifested by the broad combination of the reflected and converted waves, e.g., PP-, SS-, PS-, and SP- waves. This complexity of the wave phenomena in the elastic medium is transformed into distinct anomalies, associated with the HC reservoir and fractured zone observed in the corresponding seismograms, especially in the case of the vertical velocity.

Future research will be aimed at developing full-wave inversion algorithms based on accurate modeling of the elastic wave propagation using the GCM.

ACKNOWLEDGMENTS

This research was supported by the Russian Science Foundation, project No. 16-11-10188. The authors also acknowledge support from the University of Utah's Consortium for Electromagnetic Modeling and Inversion (CEMI) and TechnoImaging.

We are thankful to Yuriy Ivanov and two anonymous reviewers for their useful comments and recommendations which helped to improve the paper.

REFERENCE LIST

Aki K. and Richards P.G. 2002. *Quantitative seismology, theory and methods*. Second edition, University Science Books, Sausalito, California.

Berg P., If F., Nielsen P., Skovgaard O. 1994. Analytical reference solutions. *Modeling the earth for oil exploration*, 421-427.

Biryukov V.A., Miryakha V.A., Petrov I.B., and Khokhlov N.I. 2016. Simulation of elastic wave propagation in geological media: intercomparison of three numerical methods. *Computational Mathematics and Mathematical Phyisics*, **56** (6), 1086-1095.

Bording R.P. and Lines L.R. 1997. *Seismic Modeling and Imaging with the Complete Wave Equation.* SEG.

Cance P. and Capdeville Y. 2015. Validity of the acoustic approximation for elastic waves in heterogeneous media. *Geophysics*, 80(4), T161-T173.

Carcione J.M., Herman G.C. and Kroode A.P.E. 2002. Seismic modeling. *Geophysics*, **67** (4), 1304-1325.

Chapman C. 2004. *Fundamentals of Seismic Wave Propagation*. Cambridge University Press.

Di Bartolo L., Dors C. and Mansur W.J. 2012. A new family of finite-difference schemes to solve the heterogeneous acoustic wave equation. *Geophysics* **77** (5), T187-T199.

Di Bartolo L., Vieira A.P.G., Dors C., and Mansur W.J. 2015. Memory optimized acoustic-elastic FD coupling for offshore seismic simulations. *2015 SEG Annual Meeting. – Society of Exploration Geophysicists*.

Etgen J.T. and O'Brien M.J. 2007. Computational methods for large-scale 3D acoustic finite-difference modeling: A tutorial. *Geophysics* **72** (5), SM223-SM230.

Favorskaya A.V. and Petrov I.B. 2016. A study of high-order grid-characteristic methods on unstructured grids. *Numerical Analysis and Applications* **9**, 171-178.

Favorskaya A.V., Petrov I.B., Vasyukov A.V., Ermakov A.S., Beklemysheva K.A., Kazakov A.O., Novikov A.V. 2014. Numerical Simulation of Wave Propagation in Anisotropic Media. *Doklady Mathematics* **90(3)**, 778-780.

Jiang F. and Jin S. 2013. Hybrid Acoustic-elastic modeling method using adaptive grid finite difference scheme in marine environment. *75th EAGE Conference & Exhibition incorporating SPE EUROPEC 2013*.

Golubev V.I., Petrov I.B. and Khokhlov N.I. 2013. Numerical simulation of seismic activity by the grid-characteristic method. *Computational Mathematics and Mathematical Physics* **53** (10), 1523-1533.

Golubev V.I., Petrov I.B., and Khokhlov N.I. 2015. Simulation of seismic processes inside the planet using the hybrid grid-characteristic method. *Mathematical Models and Computer Simulations*, **7** (5), 439–445.

Hestholm S. 2009. Acoustic VTI modeling using high-order finite differences, *Geophysics* **74** (5), T67-T73.

Hobro J.W.D., Chapman C.H. and Robertsson J.O.A. 2014. A method for correcting acoustic finite-difference amplitudes for elastic effects. *Geophysics* **79** (4), T243-T255.

Jianfeng Z. 1997. Quadrangle-grid velocity-stress finite-difference method for elastic-wave-propagation simulation. *Geophys. J. Int.* **131** (1), 127-134.

Dumbser M., K¨aser M. and De La Puente J. 2000. Arbitrary High Order Finite Volume Schemes for Seismic Wave Propagation on Unstructured Meshes in 2D and 3D. *Geophys. J. Int* **142**.

Käser M. and Dumbser M. 2006a. An arbitrary high-order discontinuous Galerkin method for elastic waves on unstructured meshes – I. The two-dimensional isotropic case with external source terms. *Geophys. J. Int.* **166** (2), 855-877.

Käser M. and Dumbser M. 2006b. An arbitrary high-order discontinuous Galerkin method for elastic waves on unstructured meshes – II. The three-dimensional isotropic case. *Geophys. J. Int.* **167** (1), 319-336.

Käzer M. and Dumbser M. 2008. A highly accurate discontinuous Galerkin method for complex interfaces between solids and moving fluids. *Geophysics* **73** (3), T723-T725.

Käser M. and Igel H. 2001. Numerical simulation of 2D wave propagation on unstructured grids using explicit differential operators. *Geophysical Prospecting* **49** (5), 607-619.

Kholodov A.S. and Kholodov Ya.A. 2006. Monotonicity criteria for difference schemes designed for hyperbolic equations. *Computational Mathematics and Mathematical Physics* **46** (9), 1560-1588.

Kvasov I.E. and Petrov I.B. 2012. High-performance computer simulation of wave processes in geological media in seismic exploration. *Computational Mathematics and Mathematical Physics* **52** (2), 302-313

Lamb H. 1904. On the propagation of tremors over the surface of an elastic solid. *Philosophical Transactions of the Royal Society of London A: Mathematical, Physical and Engineering Sciences* **203** 1-42.

Landau L.D. and Lifshitz E.M. 1959. *Fluid mechanics*. Pergamon Press.

Levander A. 1988. Fourth-order finite-difference P-SV seismograms. *Geophysics* **53** (11), 1425-1436.

LeVeque R. 2002. *Finite volume methods for hyperbolic problems*. Cambridge University Press.

Magomedov K.M. and Kholodov A.S. 1988. *Grid characteristic methods.* Nauka, Moscow.

Matuszyk P.J. and Demkowicz L.F. 2014. Solution of coupled poroelastic/acoustic/elastic wave propagation problems using automatic hp-adaptivity. Computer Methods in Applied Mechanics and Engineering, 281, 54-80.

Muratov M.V. and Petrov I.B. 2013. Estimation of wave responses from subvertical macrofracture systems using a grid characteristic method. *Mathematical Models and Computer Simulations* **5** (5), 479-491.

Peter D., Komatitsch D., Luo Y., Martin R., Le Goff N., Casarotti E., Le Loher P., Magnoni F., Liu Q., Blitz C., Nissen-Meyer T., Basini P. and Tromp J. 2011. Forward and adjoint simulations of seismic wave propagation on fully unstructured hexahedral meshes. *Geophys. J. Int.* **186** (2), 721-739.

Petrov I.B., Favorskaya A.V., Sannikov A.V. and Kvasov I.E. 2013. Grid-Characteristic Method Using High Order Interpolation on Tetrahedral Hierarchical Meshes with a Multiple Time Step. *Mathematical Models and Computer Simulations* **5** (5), 409-415.

Sanyi Y., Shangxu W, Wenju S., Lina M. and Zhenhua L. 2014. Perfectly matched layer on curvilinear grid for the second-order seismic acoustic wave equation. *Exploration Geophysics* **45** (2), 94-104.

Seriani G., Priolo E., Carcione J.M. and Padovani E. 1992. High-order spectral element method for elastic wave modeling. 62nd Annual International Meeting and Exposition, SEG, Extended Abstracts, 1285-1288.

Solano C.A.P., Stopin A. and Plessix R.E. 2013. Synthetic study of elastic effects on acoustic full waveform inversion. *75th EAGE Conference & Exhibition incorporating SPE EUROPEC 2013*.

Tong P., Yang D. and Hua B. 2011. High accuracy wave simulation revised derivation, numerical analysis and testing of a nearly analytic integration discrete method for solving acoustic wave equation. *International Journal of Solids and Structures* **48**, 56-70.

Van Vossen R., Robertsson J.O.A. and Chapman C.H. 2002. Finite-difference modeling of wave propagation in a fluid-solid configuration. *Geophysics* **67** (2), 618-624.

Virieux J., Etienne V., Cruz-Atienza V., Brossier R., Chaljub E., Coutant O., Garambois S., Mercerat D., Prieux V., Operto S., Ribodetti A. and Tago J. 2012. *Modelling Seismic Wave Propagation for Geophysical Imaging, Seismic Waves - Research and Analysis*. Dr. Masaki Kanao (Ed.), ISBN: 978-953-307-944-8, InTech.

Wang X. and Liu X. 2007. 3-D acoustic wave equation forward modeling with topography, Appl. Geophys. **4**, 8-15.

Zeng Y.Q. and Liu Q.H. 2004. A multidomain PSTD method for 3D elastic wave equations. *Bull. seism. Soc. Am.* **94**, 1002-1015.

Zhang W., Zhang Z. and Chen X. 2012. Three-dimensional elastic wave numerical modelling in the presence of surface topography by a collocated-grid finite-difference method on curvilinear grids. *Geophys. J. Int.* **190** (1), 358-378.

Zhdanov M.S. 2002. *Geophysical Inverse Theory and Regularization Problems*. Elsevier.

Zhdanov M.S. 2015. *Inverse Theory and Applications in Geophysics*. Elsevier.

APPENDIX A: PRINCIPLES OF THE GRID-CHARACTERISTIC METHOD

The foundations of the grid-characteristic method for solving the transport equation were introduced in Magomedov and Kholodov (1988). Here we present a short overview of the mathematical principles of this method for solving the hyperbolic systems of equations with constant coefficients, following (Petrov *et al.* 2013).

The main idea of the grid-characteristic method is to use the characteristic properties of the corresponding hyperbolic system of equations, which allow us to transform the original hyperbolic system of equations, describing the wave phenomena in acoustic or elastic media, into a system of transport equations. It is well known that the solution of the transport equations at later time can be determined as a linear combination of the displacements at a certain spatial step solutions at some previous time moment, which makes it possible to construct a direct time-stepping iterative algorithm of computing the wave fields at any time moment from the initial and boundary conditions. The stability conditions for rectangular discretization grids used in this paper are of the Courant-Fridrich-Levy type for both systems of equations describing elastic and acoustic waves (Favorskaya and Petrov, 2016).

Let us consider the key mathematical principles of the GCM technique as applied to the wave phenomenon. Systems of equations (1), (2) and (3), (4) are special cases of the hyperbolic systems of equations with constant coefficients. Let us consider an arbitrary hyperbolic system of equations with constant coefficients:

$$\mathbf{q}_t(t,x,y,z) + \mathbf{A}_1\mathbf{q}_x(t,x,y,z) + \mathbf{A}_2\mathbf{q}_y(t,x,y,z) + \mathbf{A}_3\mathbf{q}_z(t,x,y,z) = 0, \qquad \text{(A1)}$$

where $\mathbf{q}(t,x,y,z)$ is a vector of the unknown fields, having J components; $\mathbf{q}_t$ denotes the partial derivative of $\mathbf{q}$ with respect to t; $\mathbf{q}_x$, $\mathbf{q}_y$ and $\mathbf{q}_z$ denote the partial derivatives of vector $\mathbf{q}$ with respect to x , y, and z, respectively; and $\mathbf{A}_1$, $\mathbf{A}_2$, and $\mathbf{A}_3$ are the given $J \times J$ matrices.

In order to apply the grid-characteristic method, we represent matrices $\mathbf{A}_k$ using their spectral decomposition. For example, for matrix $\mathbf{A}_1$ we have:

$$\mathbf{A}_1 = (\mathbf{\Omega}_1)^{-1}\mathbf{\Lambda}_1\mathbf{\Omega}_1, \tag{A2}$$

where $\mathbf{\Lambda}_1$ is a $J \times J$ diagonal matrix, formed by the eigenvalues $\Lambda_{1,j}$ of matrix $\mathbf{A}_1$; and $(\mathbf{\Omega}_1)^{-1}$ is $J \times J$ matrix formed by the corresponding eigenvectors.

Let us consider $J \times J$ matrices $\mathbf{X}_{1,j}$ determined by the following expression:

$$\mathbf{X}_{1,j} = \boldsymbol{\varpi}_{*1,j}\boldsymbol{\varpi}_{1,j}.$$

In the last formula, $\boldsymbol{\varpi}_{*1,\mathrm{j}}$ is the j's column of matrix $(\mathbf{\Omega}_1)^{-1}$, and $\boldsymbol{\varpi}_{1,\mathrm{j}}$ is the j's row of matrix $\mathbf{\Omega}_1$. Due to characteristic properties of the system of hyperbolic equations (A1), the solution of this equation, vector **q,** at the x direction can be written as follows:

$$\mathbf{q}(t+\tau, x, y, z) = \sum_{j=1}^{J} \mathbf{X}_{1,j}\mathbf{q}\big(t, x - \Lambda_{1,j}\tau, y, z\big), \tag{A3}$$

where τ is the time step of the solution.

Similar expressions can be written for the solution of equations (A1) at the y and z directions, respectively:

$$\mathbf{q}(t+\tau, x, y, z) = \sum_{j=1}^{J} \mathbf{X}_{2,j}\mathbf{q}\big(t, x, y - \Lambda_{2,j}\tau, z\big), \tag{A4}$$

$$\mathbf{q}(t+\tau, x, y, z) = \sum_{j=1}^{J} \mathbf{X}_{3,j}\mathbf{q}\big(t, x, y, z - \Lambda_{3,j}\tau\big), \tag{A5}$$

Equations (A3) – (A5) can be used to find the solution, vector **q**, at any time moment, $t + \tau$, from the given initial conditions.

Note that matrices $\mathbf{X}_{1,j}$ satisfy the following condition:

$$\sum_{j=1}^{\mathrm{J}} \mathbf{X}_{1,j} = \boldsymbol{I}.$$

Let us assume that matrix $\mathbf{A}_1$ has J_+ positive, J_- negative, and J_0 zero eigenvalues, respectively. Therefore, the sum of matrices, $\mathbf{X}_{1,j}$, corresponding to zero eigenvalues, can be expressed as follows:

$$\sum_{j\in J_0} \mathbf{X}_{1,j} = \mathbf{I} - \sum_{j\in J_+} \mathbf{X}_{1,j} - \sum_{j\in J_-} \mathbf{X}_{1,j}. \tag{A6}$$

Considering (A6), expression (A3) will take the following form:

$$\mathbf{q}(t+\tau,x,y,z) = \mathbf{q}(t,x,y,z) + \sum_{j\in J_+\cup J_-} \mathbf{X}_{1,\mathrm{j}} \left(\mathbf{q}\left(t, x-\Lambda_{1,\mathrm{j}}\tau, y, z\right) - \mathbf{q}(t,x,y,z)\right). \quad \text{(A7)}$$

In order to reduce the number of mathematical operations, the computations according to expression (A7) could be conducted in three stages.

In the first stage vector $\mathbf{q}(t,x,y,z)$ is multiplied by matrix $\mathbf{\Omega}_1$ to find vector $\boldsymbol{\omega}(t,x,y,z)$:

$$\boldsymbol{\omega}(t,x,y,z) = \mathbf{\Omega}_1 \mathbf{q}(t,x,y,z). \quad \text{(A8)}$$

In the second stage, we determine vector $\boldsymbol{\omega}(t+\tau,x,y,z)$ using the following recursive formula, which can be derived from equation (A7):

$$\boldsymbol{\omega}(t+\tau,x,y,z) = \boldsymbol{\omega}(t,x,y,z) + \sum_{l\in J_+\cup J_-} \left(\boldsymbol{\omega}\left(t, x-\Lambda_{1,l}\tau, y, z\right) - \boldsymbol{\omega}(t,x,y,z)\right), \quad \text{(A9)}$$

Where $l \in J_+ \cup J_-$.

In the third stage, vector $\boldsymbol{\omega}(t+\tau,x,y,z)$ is multiplied by matrix $(\mathbf{\Omega}_1)^{-1}$ to find the solution, vector $\mathbf{q}$, of the system of hyperbolic equations (A1):

$$\mathbf{q}(t+\tau,x,y,z) = (\mathbf{\Omega}_1)^{-1} \boldsymbol{\omega}(t+\tau,x,y,z). \quad \text{(A10)}$$

Note that, determining vector $\boldsymbol{\omega}(t,x,y,z)$ from equation (A9) is equivalent to solving the corresponding transport equation for $j \in J_+ \cup J_-$ (Petrov *et al.*, 2013):

$$\left(\omega_j\right)_t + \Lambda_{1,\mathrm{j}} \left(\omega_j\right)_x = 0, \quad \text{(A11)}$$

where *x, t* subscripts denote the partial derivatives with respect to time *x, t,* respectively.

In numerical computations, we consider the values of vectors $\mathbf{q}$ and $\boldsymbol{\omega}$ given on some discretization grid.

APPENDIX B: BOUNDARY AND INTERFACE CONDITIONS

In order to obtain a unique solution of the system of hyperbolic equations (A1), one should use the corresponding boundary conditions on the surface of the modeling domain, which, in general terms, can be written as follows:

$$\mathbf{Dq}(t+\tau, x_0, y_0, z_0) = \mathbf{d}, \tag{B1}$$

where **D** and **d** are some given matrix and vector, respectively.

For example, in a case of elastic media, two types of boundary conditions can be used. One is based on the given traction, **f**:

$$\mathbf{T} \cdot \mathbf{n} = \mathbf{f}, \tag{B2}$$

where **n** is a unit vector of the outer normal to the boundary of the modeling domain.

Another boundary condition can be based on a given velocity $\mathbf{v}_0$ at the boundary:

$$\mathbf{v} = \mathbf{v}_0. \tag{B3}$$

One can also use the first combined boundary condition for the elastic medium with the given normal projection of the velocity at the boundary, v_{n}, and a given tangential component of the traction, $\mathbf{f}_\tau$:

$$\mathbf{v} \cdot \mathbf{n} = v_{\mathrm{n}}. \tag{B4}$$

$$\mathbf{T} \cdot \mathbf{n} = \mathbf{f}_\tau, \tag{B5}$$

$$(\mathbf{T} \cdot \mathbf{n}) \cdot \mathbf{n} = 0. \tag{B6}$$

The second combined boundary condition for elastic medium is based on the given normal projection of the traction, f_{n}, and a given tangential component of the velocity at the boundary $\mathbf{v}_\tau$:

$$\mathbf{v} \cdot \mathbf{n} = 0, \tag{B7}$$

$$\mathbf{v} = \mathbf{v}_\tau, \tag{B8}$$

$$(\mathbf{T} \cdot \mathbf{n}) \cdot \mathbf{n} = f_{\mathrm{n}}. \tag{B9}$$

Let us now consider the typical interface conditions at the contact between two elastic bodies, $\boldsymbol{a}$ and $\boldsymbol{b}$, assuming that **n** is a unit vector of the outer normal to the boundary of body, a. There are two types of interface conditions. One is based on the conditions of continuity of the velocity and traction:

$$\mathbf{v}_\mathrm{a} = \mathbf{v}_\mathrm{b}, \tag{B10}$$

$$\mathbf{f}_\mathrm{a} = -\mathbf{f}_\mathrm{b}. \tag{B11}$$

One uses the free sliding conditions:

$$\mathbf{v}_\mathrm{a} \cdot \mathbf{n} = \mathbf{v}_\mathrm{b} \cdot \mathbf{n}, \tag{B12}$$

$$f_\mathrm{a,p} = -f_\mathrm{b,p}, \tag{B13}$$

$$\mathbf{f}_{\mathrm{a},\tau} = \mathbf{f}_{\mathrm{b},\tau} = 0. \tag{B14}$$

In a general case of acoustic bodies, two types of boundary conditions can be used on the surface of the modeling domain. One is based on the given pressure field, p_0:

$$p = p_0. \tag{B15}$$

This boundary condition can be calculated as follows:

$$\mathbf{v}(t+\tau, x_0, y_0, z_0) =$$

$$= \mathbf{v}_\mathrm{in}(t+\tau, x_0, y_0, z_0) + (c\rho)^{-1}(p_\mathrm{in}(t+\tau, x_0, y_0, z_0) - p_0)\mathbf{n}, \tag{B16}$$

$$p(t+\tau, x_0, y_0, z_0) = p_0. \tag{B17}$$

The other condition can be based on a given normal projection of the velocity at the boundary v_n:

$$\mathbf{v} \cdot \mathbf{n} = v_\mathrm{n}. \tag{B18}$$

This boundary condition can be calculated as follows:

$$\mathbf{v}(t+\tau, x_0, y_0, z_0) = \mathbf{v}_\mathrm{in}(t+\tau, x_0, y_0, z_0) - (\mathbf{v}_\mathrm{in}(t+\tau, x_0, y_0, z_0) \cdot \mathbf{n} - v_\mathrm{n})\mathbf{n}, \tag{B19}$$

$$p(t+\tau, x_0, y_0, z_0) = p_\mathrm{in}(t+\tau, x_0, y_0, z_0) + c\rho(\mathbf{v}_\mathrm{in}(t+\tau, x_0, y_0, z_0) \cdot \mathbf{n} - v_\mathrm{n}). \tag{B20}$$

Let us consider now the typical interface conditions at the contact between two acoustic bodies, a and b, assuming that **n** is a unit vector of the outer normal to the boundary of body a. There is only one type of mathematically correct interface condition for two acoustic bodies:

$$\mathbf{v}_{\mathrm{a}} \cdot \mathbf{n} = \mathbf{v}_{\mathrm{b}} \cdot \mathbf{n}, \tag{B21}$$

$$p_{\mathrm{a}} = p_{\mathrm{b}}. \tag{B22}$$

LIST OF CAPTIONS

Figure 1. A sketch of a Lamb test model.

Figure 2. The original seismograms obtained numerically and analytically. Lamb test model. Panel (a) – horizontal component of velocity. Panel (b) – vertical component of velocity.

Figure 3. A sketch of two half-spaces model.

Figure 4. The original seismograms obtained numerically and analytically. Two half-spaces model. Panel (a) – horizontal component of velocity. Panel (b) – vertical component of velocity.

Table 1: Parameters of the multilayed medium shown in Fig. 1

Figure 5. A sketch of a horizontally-layered model, containing a hydrocarbon (HC) reservoir (layer #7) with relatively low velocities of seismic wave propagation.

Figure 6. Snapshots of the wave propagations at 0.4514 s with the gray scale representing the amplitude of the wave velocity.. Panel (a) represents the wave propagation in the acoustic medium (Models 3 and 4), while panel (b) shows the wave propagation in the elastic medium (Models 1 and 2). The left side of each panel corresponds to the models without the HC reservoir, while the right side corresponds to the models with the HC reservoir.

Figure 7. Snapshots of the wave propagations at 0.6438 s. with the gray scale representing the amplitude of the wave velocity. Panel (a) represents the wave propagation in the acoustic medium (Models 3 and 4), while panel (b) shows the wave propagation in the elastic medium (Models 1 and 2). The left side of each panel corresponds to the models without the HC reservoir, while the right side corresponds to the models with the HC reservoir.

Figure 8. Seismograms corresponding to the vertical component of the wave velocity. Panel (a) represents seismograms computer simulated for the acoustic medium (Models 3 and 4), while panel (b) shows the corresponding seismograms for the elastic medium (Models 1

and 2). The left side of each panel corresponds to the models without the HC reservoir, while the right side corresponds to the models with the HC reservoir. The distance is plotted horizontally. The time is plotted vertically.

Figure 9. Seismograms corresponding to the horizontal component of the wave velocity. Panel (a) represents seismograms computer simulated for the acoustic medium (Models 3 and 4), while panel (b) shows the corresponding seismograms for the elastic medium (Models 1 and 2). The left side of each panel corresponds to the models without the HC reservoir, while the right side corresponds to the models with the HC reservoir. The distance is plotted horizontally. The time is plotted vertically.

Figure 10. An example of nonuniform grid with different cell sizes in different areas.

Figure 11. A sketch of a horizontally-layered background model, containing sixteen fractures.

Figure 12. A fragment of the discretization grid used for modeling the wave propagation in the medium with a fracture zone.

Figure 13. Snapshots of the wave propagations at 0.8 s with the gray scale representing the amplitude of the wave velocity.. Panel (a) represents the wave propagation in the acoustic medium, while panel (b) shows the wave propagation in the elastic medium. The left side of each panel corresponds to the models without any fracture, while the right side corresponds to the models with the fractures.

Figure 14. Seismograms representing the seismic signals for a model with fractures. Panel (a) represents seismograms for the acoustic medium, while panel (b) shows the corresponding seismograms for the elastic medium. The left panels correspond to the horizontal component of the wave velocity, while the right panels corresponds to the vertical component of the wave velocity. The distance is plotted horizontally. The time is plotted vertically.

Figure 15. Seismograms representing the difference between seismic signals obtaining in the case of fractures and in the case without any fracture. Panel (a) represents right parts of seismograms computer simulated for the acoustic medium, while panel (b) shows the corresponding right parts of seismograms for the elastic medium. The left side of each panel corresponds to the horizontal component of the wave velocity, while the right side corresponds to the vertical component of the wave velocity. The distance is plotted horizontally. The time is plotted vertically.

LIST OF TABLES

Table 1: Parameters of the multilayed medium shown in Fig. 1

The number of the layer	Density kg/m^3	P-wave velocity, m/sec	S-wave velocity, m/sec	Thickness, m
1	2100	2600	1100	60
2	2300	3200	1960	70
3	2300	3700	2260	150
4	2400	4000	2450	340
5	2500	4300	2630	360
6	2600	4500	2750	270
7	2300	3200	1700	60
8	2600	4600	2820	80
9	2700	4800	2940	70
10	2800	5400	3300	2601

Table 2: Parameters of the multilayed medium shown in Fig. 7

The number of the layer	Density kg/m^3	P-wave velocity, m/s	S-wave velocity, m/s	Thickness, m
1	2000	2170	674	500
2	2300	2130	795	100
3	2200	2500	1090	300
4	2300	2680	1220	100
5	2400	3000	1385	400
6 (with fractures))	2700	5550	3144	100
7	2800	6000	1250	150
8	2850	6000	1550	4000
Within the fractures	1350	2775	1572	–

LIST OF FIGURES

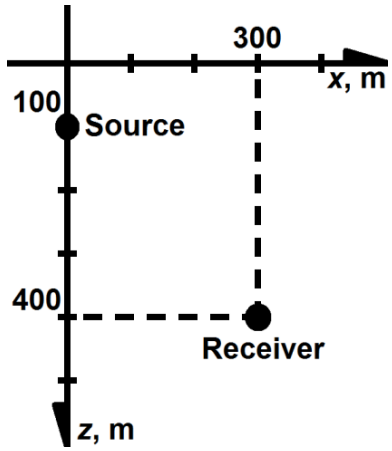

Figure 1. A sketch of a Lamb test model.

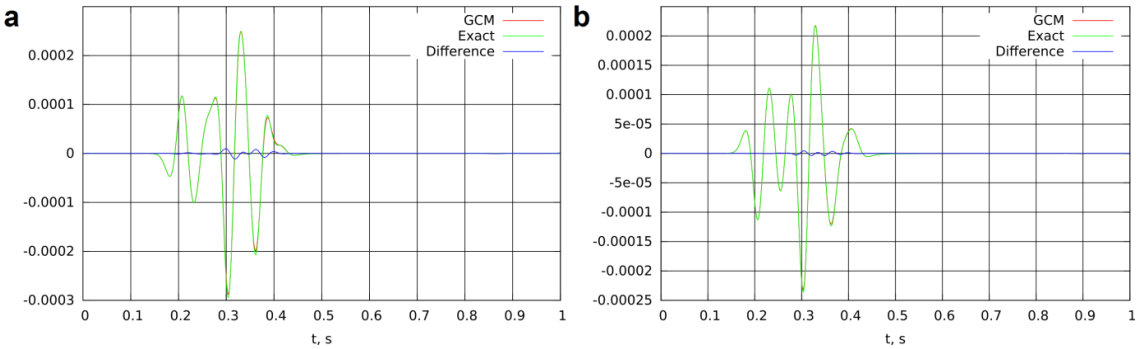

Figure 2. Seismograms obtained numerically using the grid-characterisitic method and analytically for the Lamb test model. Panel (a) – horizontal component of the velocity. Panel (b) – vertical component of the velocity.

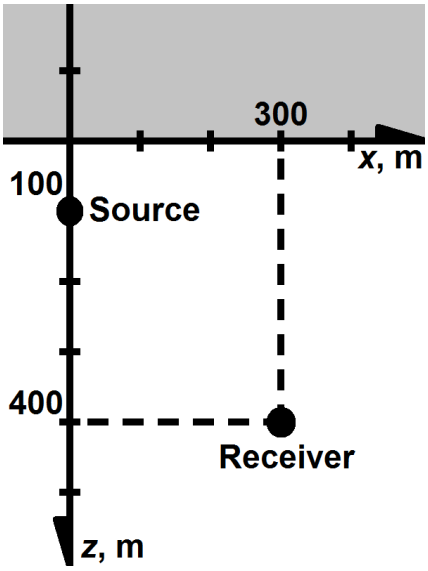

Figure 3. A sketch of two half spaces model.

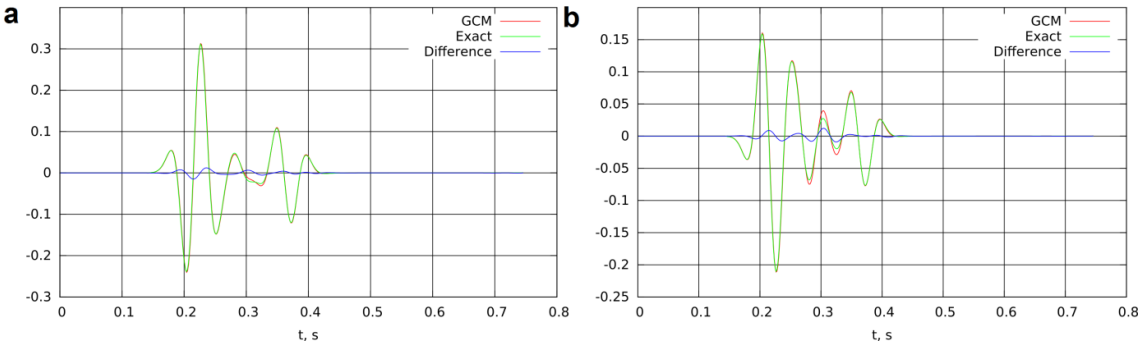

Figure 4. The original seismograms obtained numerically and analytically. for two half spaces model. Panel (a) – horizontal component of the velocity. Panel (b) – vertical component of the velocity.

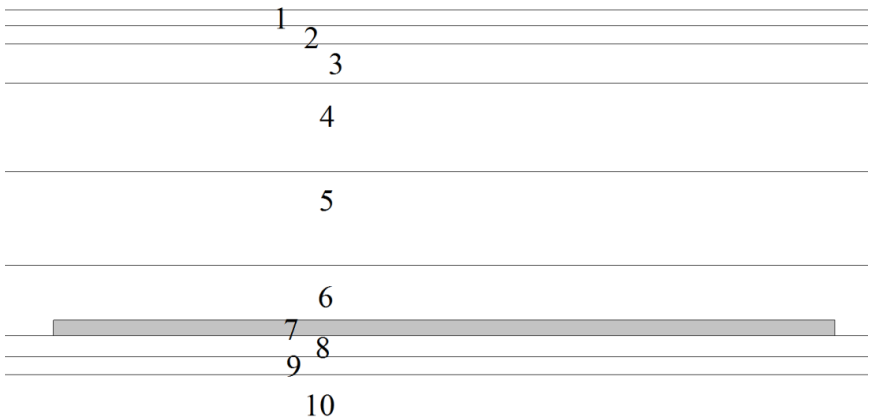

Figure 5. A sketch of a horizontally-layered model, containing a hydrocarbon (HC) reservoir

(layer #7) with relatively low velocities of seismic wave propagation.

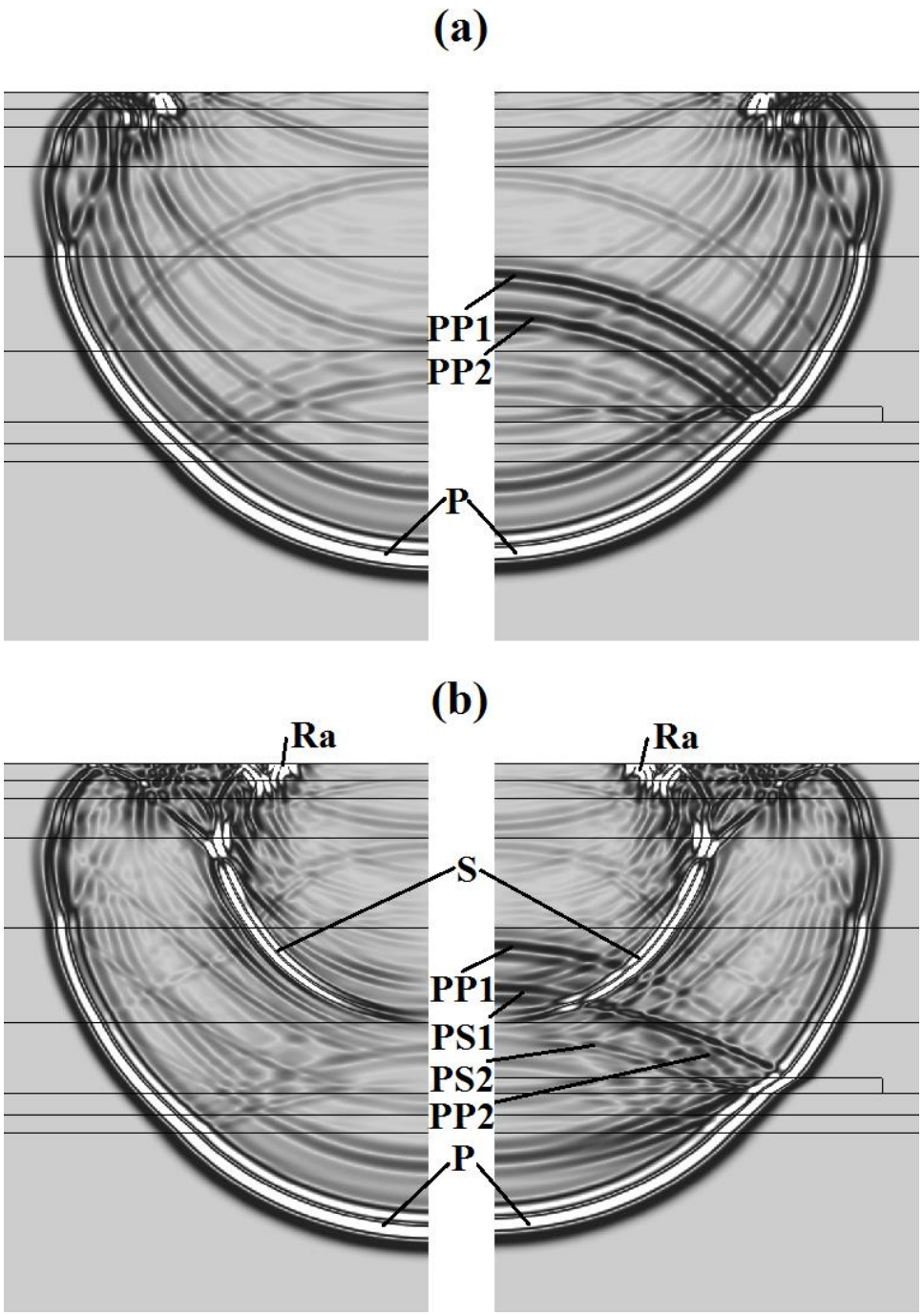

Figure 6. Snapshots of the wave propagations at 0.4514 s with the gray scale representing the amplitude of the wave velocity. Panel (a) represents the wave propagation in the acoustic medium (Models 3 and 4), while panel (b) shows the wave propagation in the elastic medium (Models 1 and 2). The left side of each panel corresponds to the models without the HC reservoir, while the right side corresponds to the models with the HC reservoir.

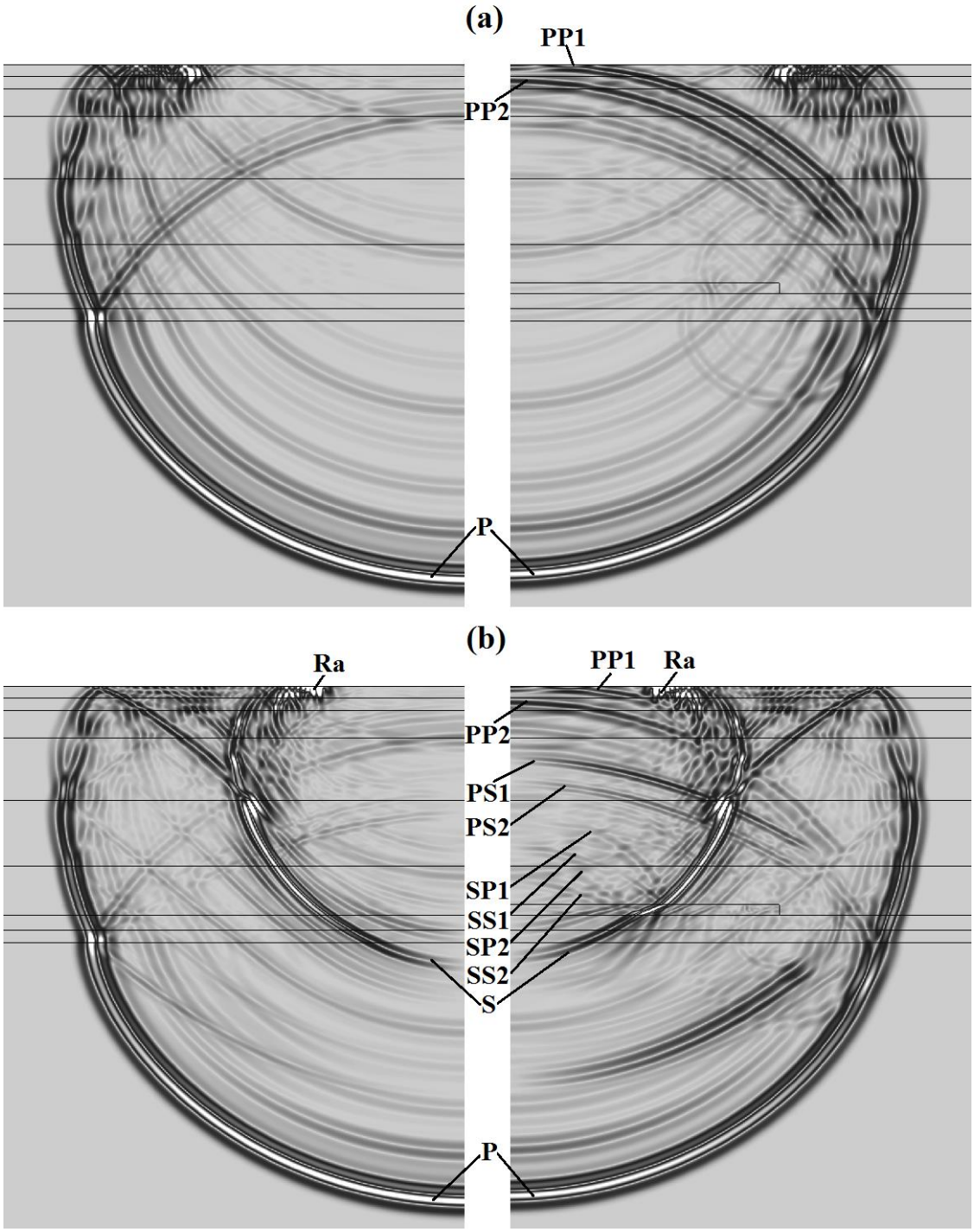

Figure 7. Snapshots of the wave propagations at 0.6438 s with the gray scale representing the amplitude of the wave velocity. Panel (a) represents the wave propagation in the acoustic medium (Models 3 and 4), while panel (b) shows the wave propagation in the elastic medium (Models 1 and 2). The left side of each panel corresponds to the models without the HC reservoir, while the right side corresponds to the models with the HC reservoir.

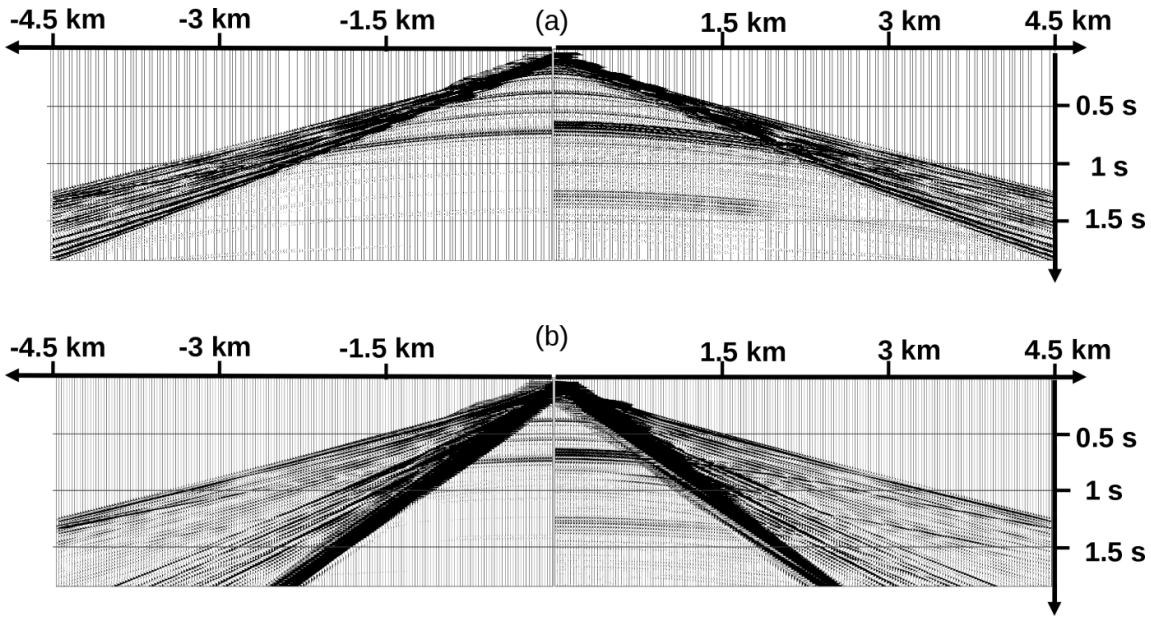

Figure 8. Seismograms corresponding to the vertical component of the wave velocity. Panel (a) represents seismograms computer simulated for the acoustic medium (Models 3 and 4), while panel (b) shows the corresponding seismograms for the elastic medium (Models 1 and 2). The left side of each panel corresponds to the models without the HC reservoir, while the right side corresponds to the models with the HC reservoir. The distance is plotted horizontally. The time is plotted vertically.

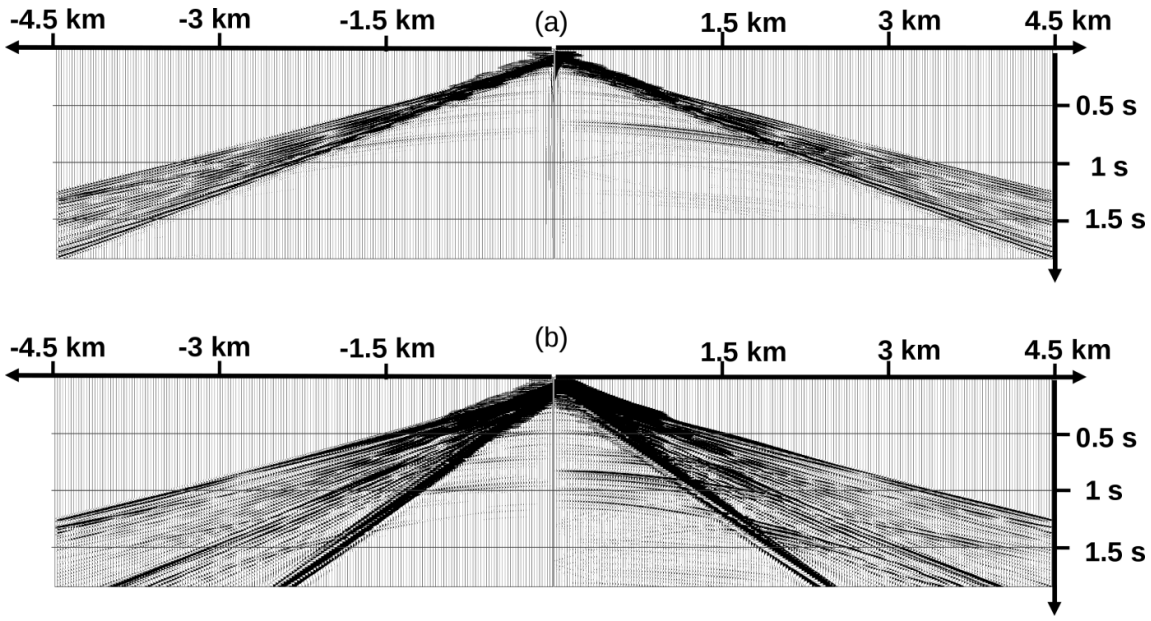

Figure 9. Seismograms corresponding to the horizontal component of the wave velocity. Panel (a) represents seismograms computer simulated for the acoustic medium (Models 3 and 4), while panel (b) shows the corresponding seismograms for the elastic medium (Models 1 and 2). The left side of each panel corresponds to the models without the HC reservoir, while the right side corresponds to the models with the HC reservoir. The distance is plotted horizontally. The time is plotted vertically.

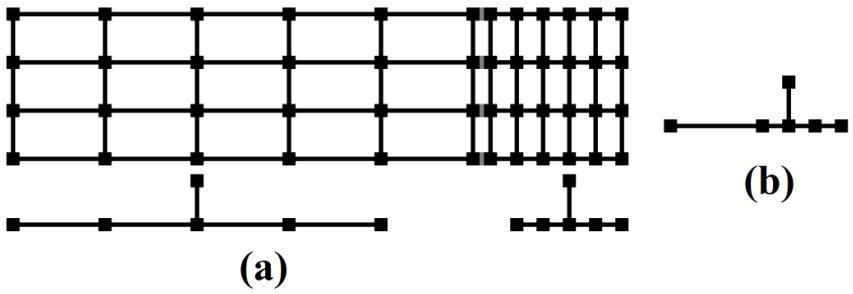

Figure 10. Example of nonuniform grid (a) with different cell sizes in different areas, and nonuniform nodes (b).

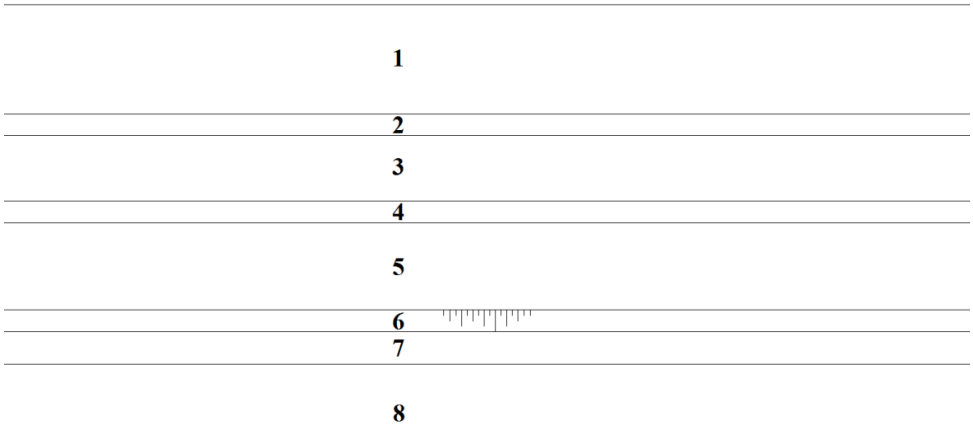

Figure 11. A sketch of a horizontally-layered background model, containing sixteen fractures.

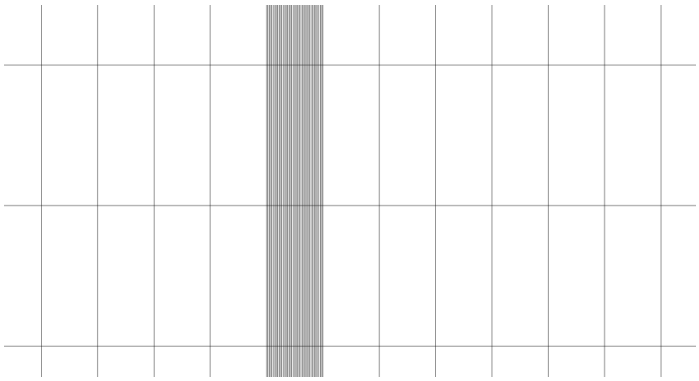

Figure 12. A fragment of the discretization grid used for modeling the wave propagation in the medium with a fracture zone.

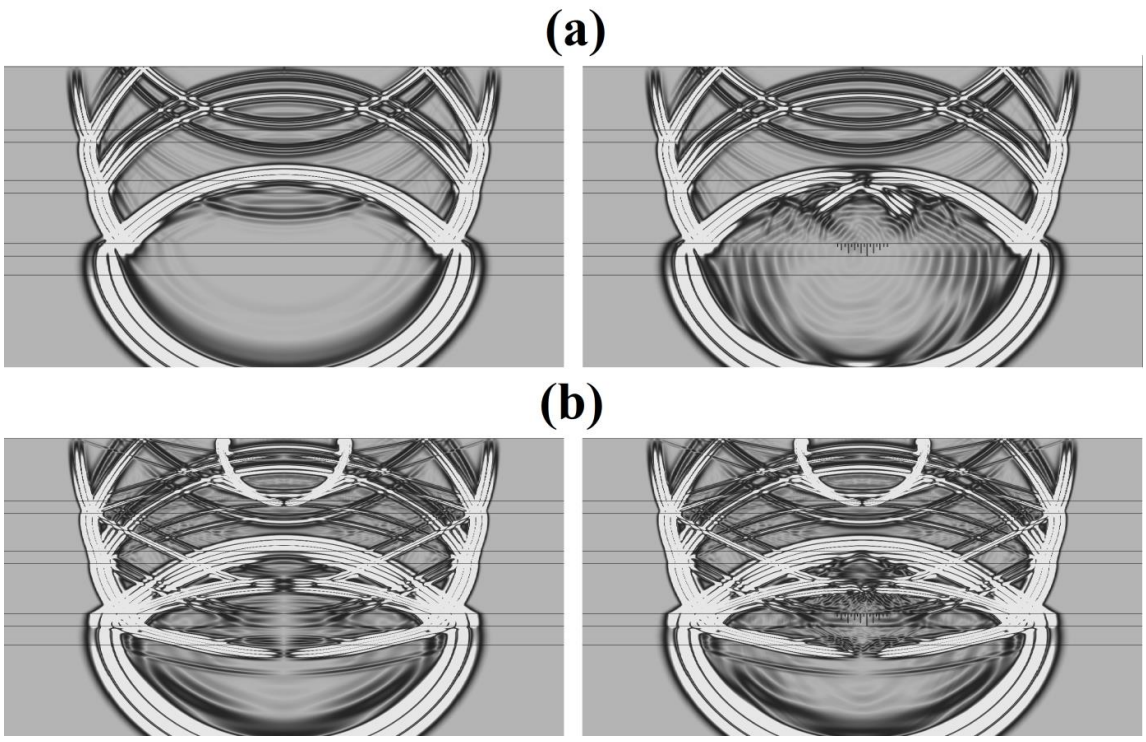

Figure 13. Snapshots of the wave propagations at 0.8 s with the gray scale representing the amplitude of the wave velocity.. Panel (a) represents the wave propagation in the acoustic medium, while panel (b) shows the wave propagation in the elastic medium. The left side of each panel corresponds to the models without any fracture, while the right side corresponds to the models with the fractures.

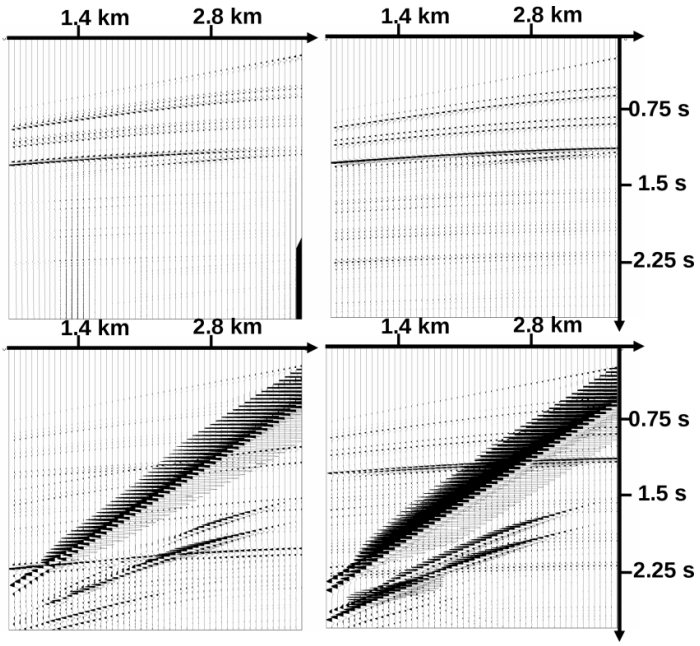

Figure 14. Seismograms representing the seismic signals for a model with fractures. Panel (a) represents seismograms for the acoustic medium, while panel (b) shows the corresponding seismograms for the elastic medium. The left panels correspond to the horizontal component of the wave velocity, while the right panels corresponds to the vertical component of the wave velocity. The distance is plotted horizontally. The time is plotted vertically.

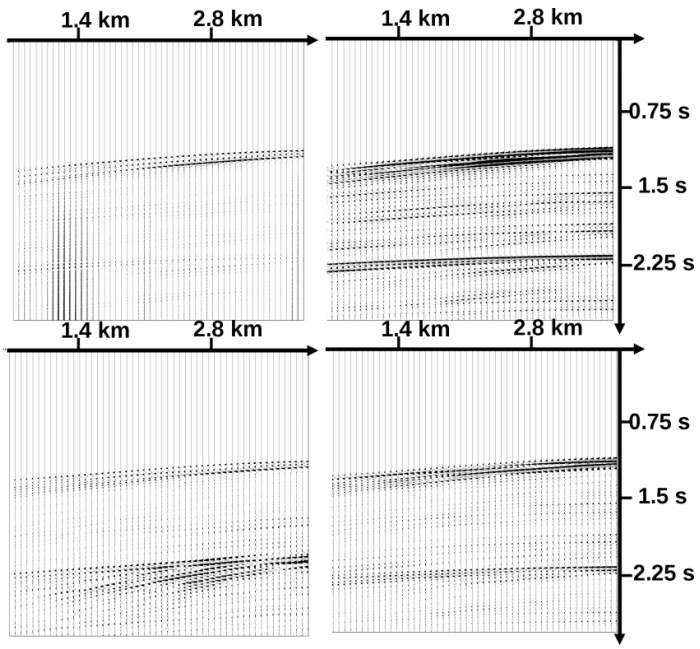

Figure 15. Seismograms representing the difference between seismic signals obtaining in the case of fractures and in the case without any fracture. Panel (a) represents right parts of seismograms computer simulated for the acoustic medium, while panel (b) shows the corresponding right parts of seismograms for the elastic medium. The left side of each panel corresponds to the horizontal component of the wave velocity, while the right side corresponds to the vertical component of the wave velocity. The distance is plotted horizontally. The time is plotted vertically.